AD-775 067

INTEGRATED OPTICS

G. Sanjiv Kamath, et al

Hughes Research Laboratory

Prepared for:

Air Force Cambridge Research Laboratories

August 1973
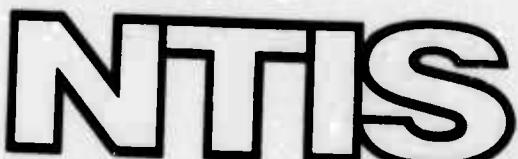
ARPA Order No. 2074

Program Code No. 3D10

Contractor: Hughes Research Laboratories

Effective Date of Contract, 1 June 1972

Contract No. F19628-72-C-0322

Principal Investigator and Phone No.
G. Sanjiv Kamath, 213 456-6411 Ext. 210

Amnon Yariv, 213 795-6841

AFCRL Project Scientist and Phone No.
Dr. Freeman D. Shepherd, Jr.   617 861-2225

Contract Expiration Date   30 November 1973
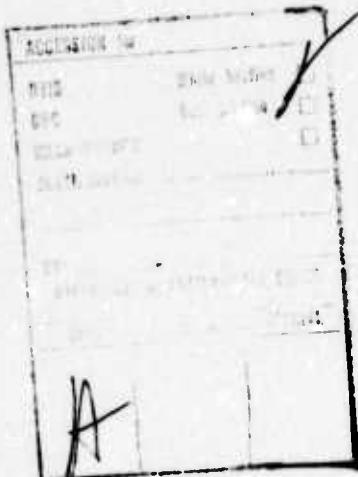
AD - 775 067

DOCUMENT CONTROL DATA · R&D		
(Security classification of title, body of abstract and indexing annotation must be entered when the overall report is classified)		

1. ORIGINATING ACTIVITY (Corporate author)	2a. REPORT SECURITY CLASSIFICATION
Hughes Research Laboratories 3011 Malibu Canyon Road Malibu, California 90265	UNCLASSIFIED
	2b. GROUP

3. REPORT TITLE

INTEGRATED OPTICS

4. DESCRIPTIVE NOTES (Type of report and inclusive dates)

Scientific.   Interim.

5. AUTHOR(S) (First name, middle initial, last name)

G. Sanjiv Kamath   Kyohei Sakuda
Amnon Yariv   Viktor Evtuhov
Michael Barnoski

6. REPORT DATE	7a. TOTAL N° OF PAGES	7b. NO. OF REFS
August 1973	78	10

8a. CONTRACT OR GRANT NO.	9a. ORIGINATOR'S REPORT NUMBER(S)
F19628-72-C-0322 ARPA Order	Semiannual Technical Report
b. PROJECT, TASK, WORK UNIT NOS. 2074	No. 2
2074 T n/a WU n/a	
c. DOD ELEMENT 61101D	9b. OTHER REPORT NO(S) (Any other numbers that may be assigned this report)
d. DOD SUBELEMENT n/a	AFCRL-TR-73-0713

10. DISTRIBUTION STATEMENT

A - Approved for public release; distribution unlimited.

11. SUPPLEMENTARY NOTES	12. SPONSORING MILITARY ACTIVITY
This research was supported by the Defense Advanced Research Projects Agency.	Air Force Cambridge Research Laboratories (LQ) LG Hanscom Field Bedford, MA 01730

13. ABSTRACT

Previous calculations of free carrier absorption and Al concentration difference between the guiding layer and the substrate required to achieve single mode propagation have been extended. In addition, the ranges of absolute Al concentration have been computed to be ~3% to 20% (minimum) for the substrate and ~0% to 17% (minimum) for the guiding layer, depending on the source wavelength to be used. Three methods of epitaxy have been used to grow layers for waveguide applications. The first multilayered structures were vapor epitaxial layers of n-type GaAs on $Ga_{0.96}Al_{0.04}As$. More than 50 layers of $Ga_{1-x}Al_xAs$ with x varying from 0 to 60% have been grown by the limited melt method. On some of these layers, a second layer with lower aluminum concentration to act as a waveguide was grown. The most significant achievement has been in the use of the infinite melt epitaxy to grow $Ga_{1-x}Al_xAs$ layers. Layers with x varying from 0 to 60% have been grown and extensively characterized for their crystal quality, chemical composition, and electrical properties. Experiments to date show that the layers have improved in their uniformity and homogeneity. Initial optical loss measurements on a vapor grown epitaxial layer of GaAs on $Ga_{1-x}Al_xAs$ have given a preliminary value of the attenuation coefficient of 2.2 cm^{-1} at 1.15 μm. Consideration has been given to the device elements for which GaAs and $Ga_{1-x}Al_xAs$ are particularly suitable. Optical filters utilizing periodic dielectric waveguides have been analyzed theoretically in detail. Computer results for the dispersion diagram of a periodically corrugated dielectric waveguide with typical parameters have been obtained.

DD FORM 1473
1 NOV 65

1

14. KEY WORDS	LINK A		LINK B		LINK C	
	ROLE	WT	ROLE	WT	ROLE	WT
GaAs						
$Ga_{1-x}Al_xAs$						
Epitaxy						
Integrated Optics						
Waveguides						
Periodic Structures						

ABSTRACT

Previous calculations of free carrier absorption and Al concentration difference between the guiding layer and the substrate required to achieve single mode propagation have been extended. In addition, the ranges of absolute Al concentration have been computed to be $\sim 3\%$ to 20% (minimum) for the substrate and $\sim 0\%$ to 17% (minimum) for the guiding layer, depending on the source wavelength to be used. Three methods of epitaxy have been used to grow layers for waveguide applications. The first multilayered structures were vapor epitaxial layers of n-type GaAs on $Ga_{0.96}Al_{0.04}As$. More than 50 layers of $Ga_{1-x}Al_xAs$ with x varying from 0 to 60% have been grown by the limited melt method. On some of these layers, a second layer with lower aluminum concentration to act as a waveguide was grown. The most significant achievement has been in the use of the infinite melt epitaxy to grow $Ga_{1-x}Al_xAs$ layers. Layers with x varying from 0 to 60% have been grown and extensively characterized for their crystal quality, chemical composition, and electrical properties. Experiments to date show that the layers have improved in their uniformity and homogeneity. Initial optical loss measurements on a vapor grown epitaxial layer of GaAs on $Ga_{1-x}Al_xAs$ have given a preliminary value of the attenuation coefficient of 2.2 cm^{-1} at 1.15 μm. Consideration has been given to the device elements for which GaAs and $Ga_{1-x}Al_xAs$ are particularly suitable. Optical filters utilizing periodic dielectric waveguides have been analyzed theoretically in detail. Computer results for the dispersion diagram of a periodically corrugated dielectric waveguide with typical parameters have been obtained.

3

TABLE OF CONTENTS

Preceding page blank

LIST OF ILLUSTRATIONS

7

Preceding page blank

I. INTRODUCTION AND SUMMARY

The objectives of this contract are to study and
analyze the propagation, attenuation, and modulation of
coherent optical waves in thin film waveguides, in particu-
lar epitaxial semiconductor structures at a wavelength of
8500 Å, to determine the parameters controlling the solution
regrowth epitaxy of the $Ga_{1-x}Al_xAs$ system, to study the
influence of the index discontinuity and semiconductor car-
rier concentration on optical properties, and to develop the
elementary optical device elements.

This report covers the work performed during the period
of January 1973 through June 1973. The present program may
be viewed as consisting of the following elements: (1) es-
tablishment of epilayer material and structure requirements
from the device point of view, (2) development of materials
growth techniques, (3) materials evaluation, and (4) device
analysis and fabrication techniques. The first element
involves the establishment of the required values of param-
eters such as free carrier absorption and other losses,
index differences required for waveguiding, and absolute Al
concentration. The materials growth techniques involve
slide-bar and vertical dipping liquid phase epitaxy and
vapor phase epitaxy. Materials evaluation includes micro-
probe, photoluminescence and x-ray analysis, Hall effect
and C-V measurements, and determination of waveguiding
properties and losses of the films. The last element of
the program is directed toward establishing specific
materials requirements for integrated optics devices and
development of fabrication techniques for rudimentary devices.
For this task some of the company-supported efforts in
specific device areas are especially helpful.

9

A. Establishment of Requirements

Consideration has been given to primarily three factors affecting waveguiding: free carrier absorption and its effect on propagation losses, difference in Al concentration between the guiding layer and the substrate required to achieve single mode propagation, and absolute Al concentration required to minimize band-to-band absorption at various wavelengths. The first two factors have been considered earlier. These calculations recently have been further refined. The ranges of absolute Al concentration have been computed to be $\sim 3\%$ to 20% (minimum) for the substrate and $\sim 0\%$ to 17% minimum for the guiding layer depending on the source wavelength to be used. Further data on the absorption in the long wavelength tail of the band edge of GaAs have been obtained from the literature. It is clear from these data that adequately low absorption coefficients are possible in good samples of GaAs. However, in situ measurements are required before an accurate value for the loss coefficient in $Ga_{1-x}Al_xAs$ waveguide structures can be obtained.

B. GaAs and $Ga_{1-x}Al_xAs$ Epitaxial Layer Growth

During the reporting period three methods of epitaxy have been used to grow layers for waveguide applications. The first multilayered structures were vapor epitaxial layers of n-type GaAs on $Ga_{0.96}Al_{0.04}As$. Cleaved rectangular pieces were made from some of these structures and waveguiding studies made on them. Based on our observations on these layers, improvements are being made in the growth techniques. More than 50 layers of $Ga_{1-x}Al_xAs$ with x varying from 0 to 60% have been grown by the limited melt method to familiarize ourselves with the mechanics of the graphite slide-bar assembly and the influence of the process parameters on the layers grown. On some of these layers, we also succeeded in

10

growing a second layer, with lower aluminum concentration, to act as a waveguide. The layers need to be improved both in the interface and in bulk uniformity. Several improvements in processing and slide-bar geometry have been made, and rapid improvements are expected in the quality of our layers. Our most significant achievement has been in the use of the infinite melt epitaxy to grow $Ga_{1-x}Al_xAs$ layers. Layers with x varying from 0 to 60% have been grown and extensively characterized for their crystal quality, chemical composition, and electrical properties. The method looks promising for the fabrication of large area $Ga_{1-x}Al_xAs$ substrates that could provide an ideal base for integrated optics technology involving gallium arsenide.

C.   Materials Evaluation

Evaluation of the $Ga_{1-x}Al_xAs$ layers grown under the various growth regimes, including infinite melt and limited melt techniques, is being carried out by determining the Al profile by electron microprobe on cleaved cross sections through the epilayers. Experiments to date show that the layers have improved in their uniformity and homogeneity. Aluminum concentration gradient across the epitaxial layer grown by the infinite melt technique has been found to be considerably smaller than for layers grown by the limited melt (slide-bar) technique. The infinite melt method gives essentially the same concentration variation in 27 µm as the slide-bar method gives in 4 µm. It is felt that the concentration variation can be reduced even further.

The layers have been examined using the scanning electron microscope as well as an optical microscope. The values of layer thickness obtained by these two techniques are in agreement. Hall measurements indicated carrier concentrations ranging from 4×10^{16} cm^{-3} to 4.5×10^{17} cm^{-3} and mobilities ranging from 93 cm^2/V-sec for p-type material to 2950 cm^2/V-sec for n-type material.

11

Initial optical loss measurements on a vapor grown epitaxial layer of GaAs on $Ga_{1-x}Al_xAs$ have been attempted Although there was a large amount of scattering in the data these initial measurements indicate that the attenuation coefficient at 1.15 μm is approximately 2.2 cm^{-1}.

Optical waveguiding also has been observed through approximately 2 mm of $Ga_{0.98}Al_{0.02}As$ liquid phase epitaxial waveguide on a substrate of $Ga_{0.95}Al_{0.05}As$. The guide thickness was 2 to 3 μm.

D.   Device Elements

During this reporting period we have begun considering device elements for which GaAs and $Ga_{1-x}Al_xAs$ are particularly suitable with the aim of establishing the relationship between device requirements and material and structure characteristics. Such components as waveguide bends and couplers, distributed feedback injection lasers, integrated detectors, modulators, and periodic optical filters have been considered in a preliminary fashion. Optical filters have been analyzed theoretically in more detail. Computer results for the dispersion diagram of a periodically corrugated dielectric waveguide with typical parameters have been obtained. The behavior of the waveguide near the important Bragg regime, where the corrugation period is equal to one-half wavelength was studied in detail. Periodic optical structures are expected to play an important role in applications such as optical filters, grating air-waveguide couplers, directional couplers, and distributed feedback lasers.

II. DEFINITION OF EPILAYER MATERIAL AND STRUCTURE REQUIREMENTS

Work on the establishment of the basic requirements imposed by the need to achieve efficient propagation in waveguides continued during this reporting period. In the course of the program consideration has been given to primarily three factors affecting waveguiding: free carrier absorption and its effect on propagation losses, difference in Al concentration between the guiding layer and the substrate required to achieve single mode propagation, and absolute Al concentration required to minimize band-to-band absorption at various wavelengths. The first two factors have been considered earlier. These earlier calculations recently have been refined further. The approximate ranges of absolute Al concentration for the substrate and the guiding layer for various source wavelengths also have been computed using the data available to date.. As new data become available, however, these calculations are likely to need updating and refinement.

A. Requirements on the Al Concentration Difference Between the Guide and the Substrate

The aluminum concentration difference between the guiding layer and the substrate required for single mode propagation was determined first in a straightforward but somewhat approximate fashion by ignoring the slight non-linearity in the dependence of the refractive index on Al concentration. We assumed in these calculations the following relationship between layer-substrate index difference, $(n_2 - n_3)$ and Al concentration difference, Δx: $n_2 - n_3 \approx 0.4 \Delta x$ where n_2 and n_3 are the guiding layer and the substrate indices of refraction, respectively.

13

The approximate condition for propagation of the first m modes at wavelength λ_o in a waveguide of height t is

$$(n_2^2 - n_3^2) \geq \left[\frac{(2m - 1) \lambda_o}{4t} \right]^2 , \quad m = 1,2,3... \quad .$$

Relating $(n_2 - n_3)$ to Al concentration difference Δx yields the condition for lowest order mode propagation

$$\frac{11.25}{n} \left(\frac{\lambda_o}{4t} \right)^2 > \Delta x > \frac{1.25}{n} \left(\frac{\lambda_o}{4t} \right)^2 ,$$

where $n = (1/2) (n_2 + n_3)$. This relation can be used to plot the curves of Fig. 1, which give the ranges of guiding film thickness and aluminum concentration difference allowed for single mode propagation.

A more accurate calculation of the relationsip between the film thickness and the Al concentration difference has also been performed. In this calculation the Sellmeier equation[1] was used to estimate the refractive indices of $Ga_{1-x}Al_xAs$ for different values of x:

$$n(x) = A + \frac{B}{\lambda_o^2 - C(x)} - D(x) \lambda_o^2$$

where the coefficients A, B, C, and D are given in Table I. A plot of the refractive index as a function of x is shown in Fig. 2 while the change in refractive index $\Delta n = n_2 - n_3$ is shown in Fig. 3. The ratio of thickness to wavelength for the first two modes of the waveguide structure is plotted in Fig. 4 as a function of concentration difference Δx between the guide and the substrate for guiding epilayer

---

[1] J.T. Boyd, IEEE J. Quantum Electron. QE-8, 788 (1972).

14

TABLE I

Refractive Index of $Ga_{1-x}Al_xAs$

$$n^2 = A + \frac{B}{\lambda^2 - C} - D\lambda^2$$

Material	A	B	C	D
GaAs	10.906	0.97501	0.27969	0.002467
$Ga_{1-x}Al_xAs$	10.906 - 2.92x	0.97501	$(0.52886 - 0.735x)^2$ $x \leq 0.36$ $(0.30386 - 0.105x)^2$ $x \geq 0.36$	0.002467 (1.41x + 1)

T980

15
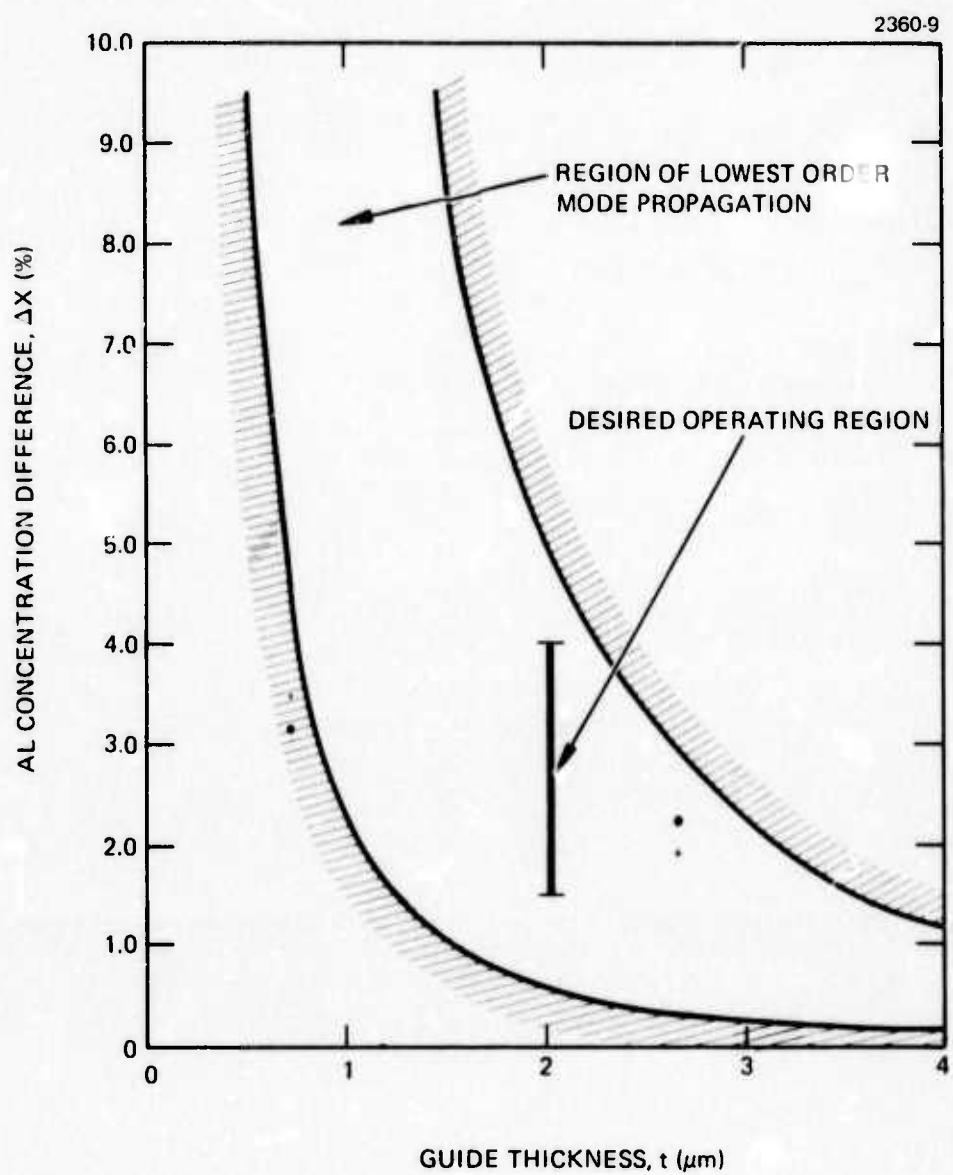
Fig. 1. Al concentration difference for
single-mode propagation (λ = 1 μm).
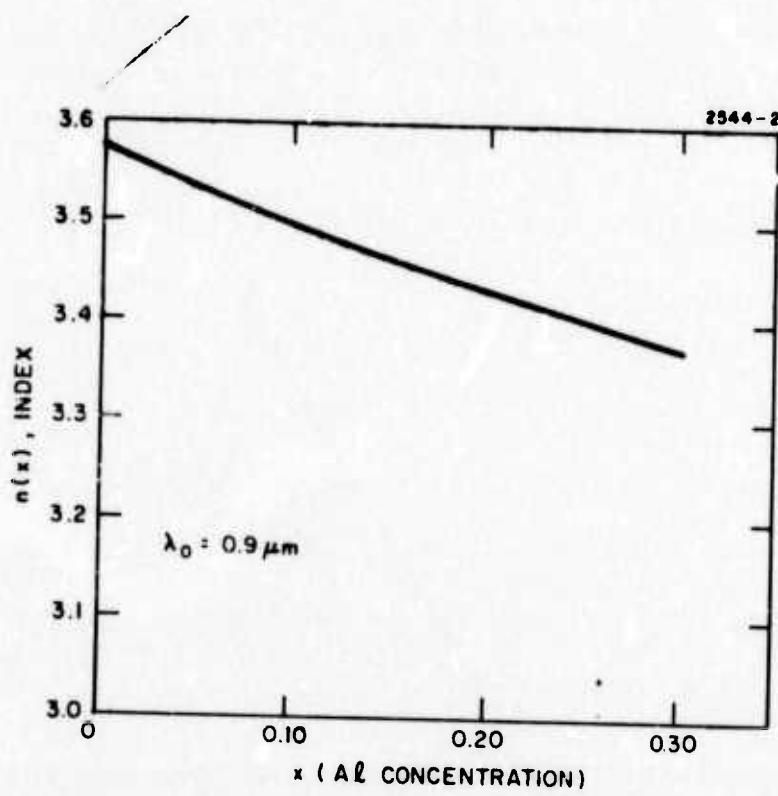
Fig. 2. Index of Refraction of $Ga_{1-x}Al_xAs$ as a function of Al concentration.
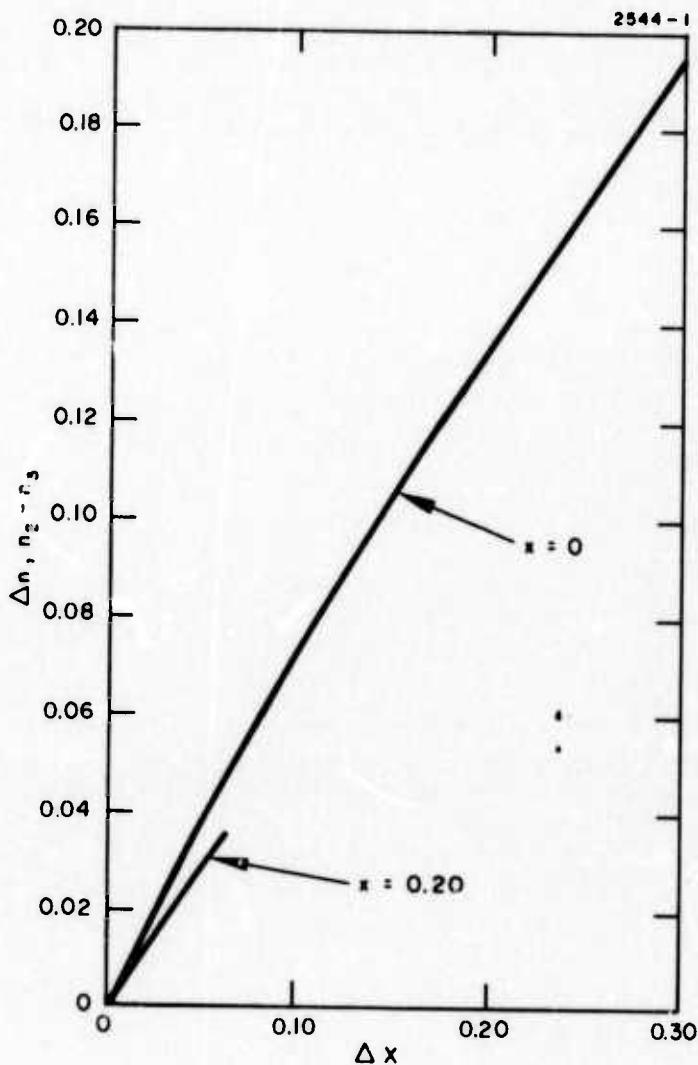
Fig. 3.
Refractive index difference as a
function of Al concentration differ-
ence between two layers of $Ga_{1-x}Al_xAs$
for two values of absolute Al
concentration.
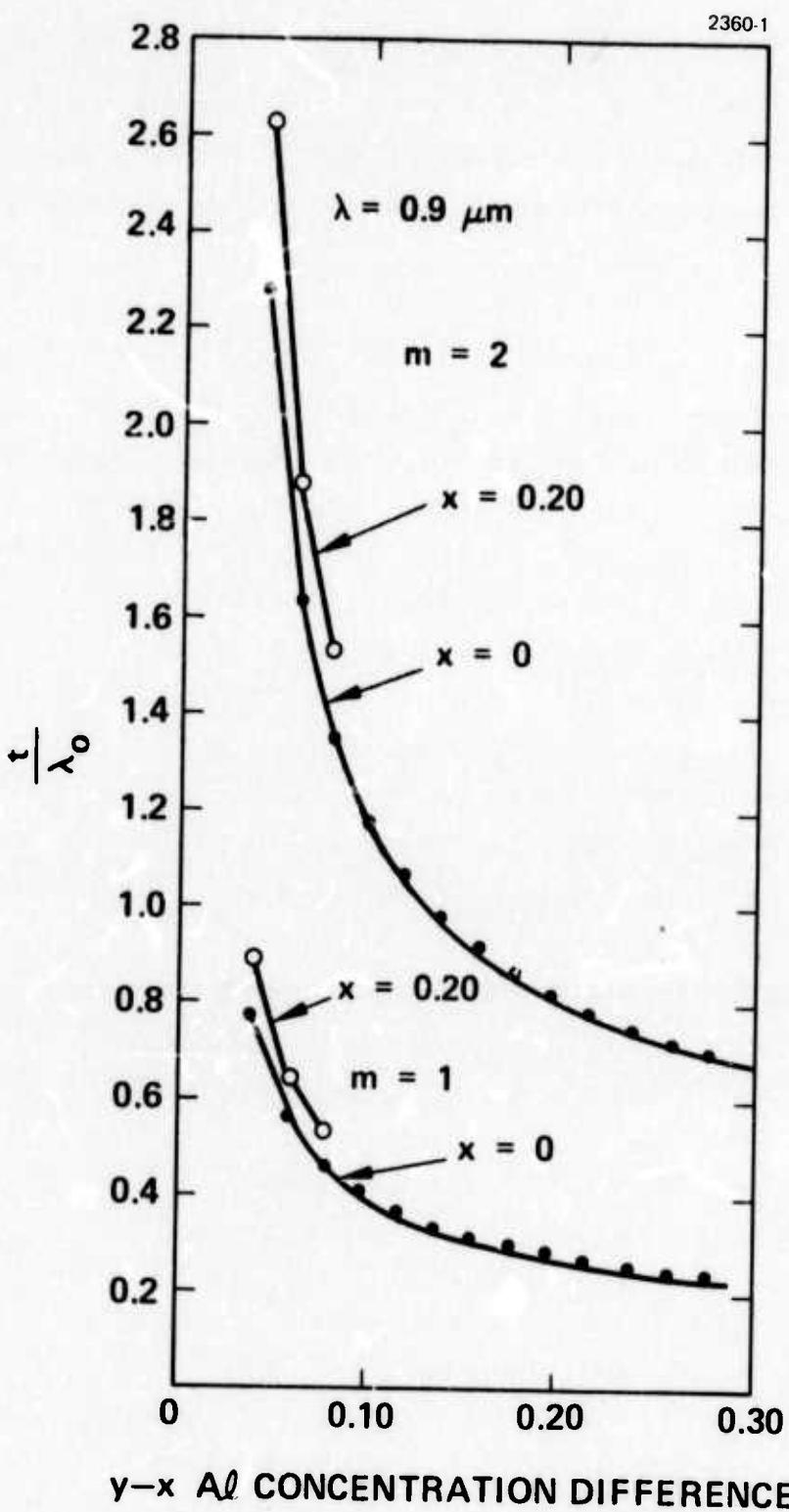
Fig. 4.
Guide thickness to wavelength
ratio as a function of Al concen-
tration between layer and substrate.

concentrations of x = 0 and x = 0.20. It is seen that although the guide thickness is dependent primarily on Al concentration difference Δx, some dependence on the absolute Al concentration is exhibited.

B.   Absolute Al Concentration Requirements

The absolute level of Al concentration in the guiding layer was estimated by considering the spectral location and shape of the $Ga_{1-x}Al_xAs$ absorption edge as a function of Al concentration and assuming a value for maximum allowable absorption coefficient due to interband transitions. Curves of Fig. 5 were plotted using available data for GaAs. The absorption edges shown for increasing Al concentrations were obtained by calculating the bandgap using the expression[2] $E_g(x) = 1.439 + 1.042 x + 0.468x^2$ and then shifting the band edge of GaAs to correspond to the computed value $E_g(x)$. The required Al concentration was determined from these curves using an allowable value of absorption coefficient $\alpha = 2$ cm^{-1} and various possible source wavelengths which might potentially be used in integrated optical circuits. The results are shown in Table II. The value of $\alpha = 2$ cm^{-1} was used because no reliable data are available for lower absorption coefficients. Therefore, the values of Al concentration given in Table II are only estimates and may tend to be low.

The material requirements established to date are summarized in Table III. Presently these are being used by the crystal growers as guidelines in establishing proper growth conditions. One of the most important properties of $Ga_{1-x}Al_xAs$ to be more accurately established is its absorption in the vicinity of the band edge as a function of Al concentration.   This not only will determine the absolute Al

---

[2] J. Shah, B. Miller, and A. DiGiovanni, J. Appl. Phys. **43**, 3436 (1972).
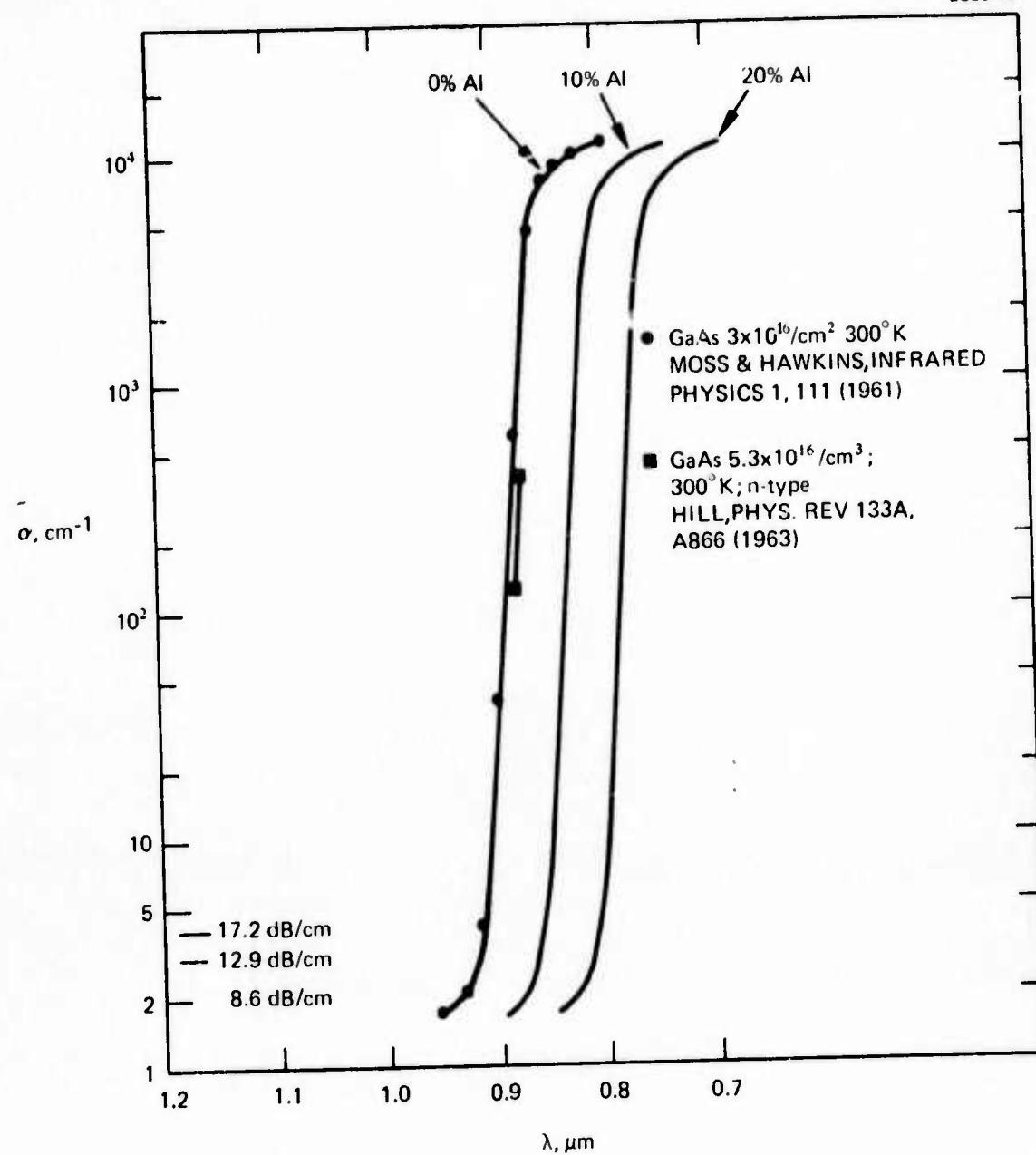
Fig. 5. Interband absorption as a function of wavelength and Al concentration.

TABLE II

Absolute Al Concentration Requirements

Take $\alpha = 2 \text{ cm}^{-1}$

Source Wavelength		Required Al Concentration in the Guide
0.85 μm	$Ga_{1-x}Al_xAs$	∿17% minimum
0.9 μm	GaAs	∿ 7% minimum
0.95 - 1.0 μm	Si:GaAs	0%

Substrate concentration ∿3% higher

Material becomes indirect at ∿40% Al

T981

TABLE III

Summary of Requirements

Impurity Concentration

$$N \leq 10^{17} \text{ cm}^{-3}$$

Al Concentration Difference Between Substrate and Guiding Layer

Δx: 1.5 to 3.5%

t: 1.25 to 2.5 μm

Absolute Levels of Al Concentration

Substrate ∿3% - 20% minimum

Guiding Layer ∿0% - 17% minimum

T982

22

concentrations required more accurately than we have done so far, but will determine the flexibility with which integrated optical circuits ultimately can be constructed. In the absence of data on GaAlAs further data on the absorption in the long wavelength tail of the band edge of GaAs has been obtained from the literature.[3] The results are plotted in Fig. 6. As can be seen, the absorption at levels below 4 cm^{-1} varies substantially from specimen to specimen which is presumably a result of impurities. It is clear from these data that adequately low absorption coefficients are possible in good samples of GaAs. However, in situ measurements are required before an accurate value for the loss coefficient in $Ga_{1-x}Al_xAs$ waveguide structures can be obtained.

---

[3] M.D. Sturge, Phys. Rev. 127, 768 (1962).
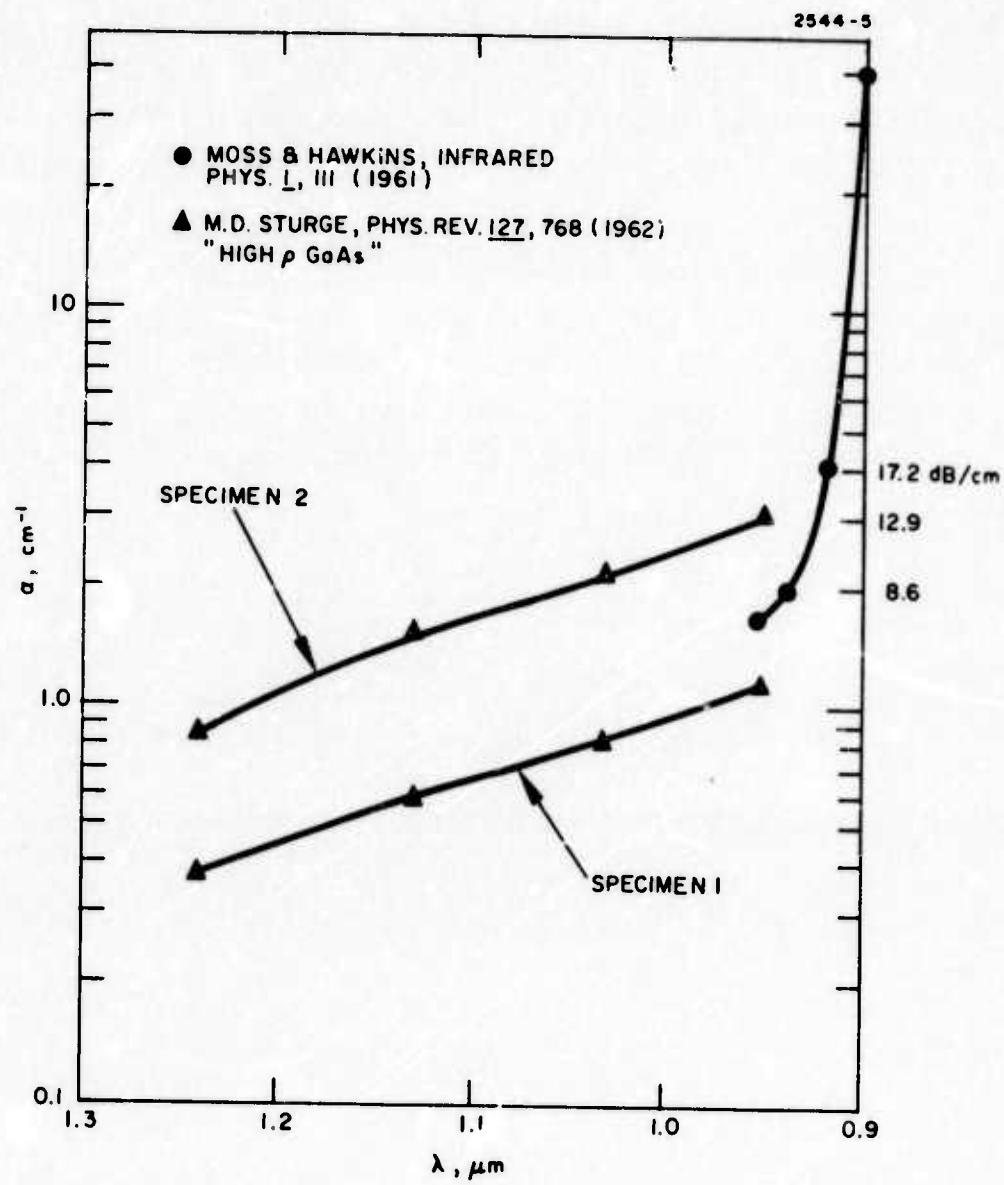
Fig. 6.
Absorption in the long wavelength tail of the GaAs
band edge.

24

III. MATERIALS GROWTH

Three approaches are being used to produce waveguide structures: vapor epitxy, limited melt (graphite slide-bar) epitaxy, and infinite melt liquid epitaxy. Each of these has its advantages, and we feel the judicious use of all three methods is essential to provide a total capability for optimizing the materials technology for integrated optics. The progress in the three areas is detailed in the following sections.

A. Vapor Epitaxy

The initial work in vapor epitaxy was described in our last report. Several additional n-type layers were grown on $Ga_{1-x}Al_xAs$ with an aluminum concentration of about 4%. The preparation of the structures for waveguiding involves the fabrication of small rectangular pieces with optically smooth cleaved edges with minimum number of imperfections or potential scattering centers in the waveguiding layer, as well as the bounding interfaces. To obtain these the epitaxial wafers were thinned down by polishing to below 6 mil total thickness and several cleaved pieces made. These were subsequently used in waveguiding experiments described in Section IV-B.

It is evident from our results that a vapor epitaxial system with more sophisticated temperature and gas-flow controls is required. Such a system has been built and is being tested. Results on layers obtained will be given in the next report.

The vapor episystem cannot be used easily to grow $Ga_{1-x}Al_xAs$ layers because of the high reactivity of aluminum. The liquid epitaxial method, however, has been used extensively for growing device quality layers of $Ga_{1-x}Al_xAs$ in several laboratories. The variant normally used is the graphite

25

slide-bar method described in our previous report. Since
with this method a small amount of melt normally is used
for individual runs, we refer to it as the limited melt
approach, as distinct from the infinite melt crystal-
pulling type technique.

B.   Limited Melt Liquid Epitaxy

The system used in our growth experiments and the
basic theory behind the process have been described pre-
viously. We have since added a temperature programmer that
enables us to control the cooling cycle reproducibly.

The boat containing the substrate and the melt was
made of high purity ultracarbon graphite. Several experi-
ments demonstrated that the softness of the graphite results
in some powder formation during the operation of the slide
bar, especially in the presence of fine crystallites of gal-
lium arsenide that tend to be dragged along with the melt.
These particles in turn scratch the grown surface. This is
highly undesirable for the growth of high quality layers,
especially when their thickness has to be very small (about
2 µm) to ensure single mode guiding. We have now begun using
a denser form of graphite (Poco graphite) which seems to have
eliminated most of the problems associated with powdered
graphite. We have gained enough experience from using these
assemblies to enable us to design a slide-bar assembly
coated with pyrolytic graphite. The use of the pyrolytic
coating guarantees smooth mechanical functioning of the
boat and minimizes contamination due to reaction with the
melt.

Using the poco graphite boat and the new temperature
controller and programmer, we have succeeded in making
several layers of $Ga_{1-x}Al_xAs$ on GaAs with about 5% Al.
The optimization of the rate of cooling has resulted in a
layer that has a more gradual variation in the Al profile

26

in the grown layer than has been previously obtained. It also has produced a layer that is more uniform in thickness and a surface that is smooth and free from major growth patterns. We have succeeded in growing a second layer with 2% Al, thus giving us a structure with a waveguiding layer. Experiments in guiding with these layers have demonstrated that they do have the necessary refractive index variation. The second layer, however, still is not free from problems. Since it has to be only about 2 to 3 microns in thickness, all control problems are exaggerated and the layers examined have been lossy.

Our calculations suggest that the guiding performance can be improved considerably by going to a higher Al content in the two layers. Increasing the Al concentration, however, poses considerable problems because of the high segregation coefficient of Al at the temperatures commonly used in epitaxial growth. The segregation coefficient varies from 20 to 30 in the temperature range of interest (800 to 900°C). We are presently using two approaches to this problem: (1) choosing proper processing conditions in the slide-bar method, and (2) using the infinite melt approach detailed later in this report.

The processing in the slide-bar assembly mainly depends on the following factors: (1) the initial temperature at which the melt is saturated, (2) the time of saturation, (3) the extent of supersaturation at the start of growth, (4) the temperature interval ΔT through which the supersaturated melt is cooled in contact with the substrate, and (5) the rate at which the melt is cooled. The details of the theoretical approach involving these parameters were given in our last report. It is important, however, to realize that each graphite assembly with its position in the dynamic gas flow tube in the furnace must be optimized for operation more or less empirically using the theory as

27

a guide. An example of such an approach with some of the relevant parameters is given in Table I.

The series of runs summarized in the table demonstrates the importance of several parameters. It can be seen, for example, that the melt must be saturated at a temperature about 7°C higher than that for starting growth. The etchback that takes place without such a precaution can be seen by cleaving and etching the grown layer and appears as a double junction (see Fig. 7). Such a regrowth is not always undesirable. In some experiments where crystal perfection is of the essence a controlled etchback and growth is known to improve epitaxial growth. However, it is important to take the possibility of etchback fully into account, to permit the growth of layers as thin as 2 μm reproducibly. In the growth of structures for waveguides the growth of the second layer with the higher refractive index is critically affected by this consideration. Therefore, it is imperative that the time rate of layer growth and the etchback and regrowth cycles, be fully integrated into the operational cycle. Unfortunately, the control of a cycle of this type is highly dependent on the position of the slide-bar assembly in the growth chamber.

Another factor brought out by the series in the table concerns the scratches in the surface of the grown layer (see Fig. 11). When the growth cycle is finalized and the mechanical tolerances of the wiping assembly in the slide bar are optimized, the close tolerances involved result in some scratching of the surface. The scratches are aggravated when the graphite tends to be powdery. The present series was accomplished with a slide-bar assembly of Ultracarbon graphite. Using the Poco graphite assembly has resulted in a considerable improvement, and the pyrolytic graphite coated assembly which we received recently is expected to eliminate

28

the scratches completely. The scratching problem is naturally aggravated on layers of small thickness, less than 3 to 4 μm.

Several of the factors mentioned above are illustrated by the series of photographs in Figs. 7 through 11. Figures 7 and 8, which correspond to samples 0040 and 0042 in Table IV, show the regrowth area in 0040 and its absence in 0042. The regrowth area can be seen better (Figs. 9 and 10) in samples 0055 and 0056 (not listed in Table IV) in a new graphite assembly. Sample 0056 was prepared using longer time of growth than sample 0055. The results show that increased time of growth only increases the thickness of the grown layer but does not affect the regrowth layer. Figure 11 shows a typically grown layer with faint scratch lines caused by particles dragging across the face.

The slide-bar assembly method has been used successfully to make a multilayer structure with $Ga_{0.98}Al_{0.02}As$ on top of $Ga_{0.96}Al_{0.04}As$. The top layer is about 5 μm thick and the bottom layer is about 6 to 8 μm thick. The quality of the layers still suffers from the defects mentioned before and the waveguiding is possible only with considerable propagation loss due to surface irregularities and imperfections.

As mentioned before, it would be desirable to increase the aluminum concentration to about 25% to improve waveguide transmission. Considering the high segregation coefficient of Al in a gallium solution, we felt that the infinite melt approach would have considerable merit for waveguide fabrication. One final point needs to made, however, about the limited melt growth with specific reference to the growth of $Ga_{1-x}Al_xAs$ layers. This concerns the variation of the segregation coefficient of Al as a function of temperature. As evident from the literature and calculations given in our previous report, the segregation coefficient increases as the growth temperature decreases. As a result, there are two factors that influence the aluminum concentration

29

TABLE IV

Epitaxial Films: Limited Melt Growth

Substrate	Melt[a] Composition, Weight in Grams			Temperature, °C		Time, t minutes[e]	Cooling Rate, ΔT/t	d,[f] μm	Growth Rate, d/t	Saturation Cycle			Remarks
	Ga	GaAs	Al	T_{sat}[c]	ΔT[d]					Time in Hours	T, °C	T_{ss}, °C[b]	
0039	1.5	0.6	0.082	891	5.5	20	0.275	4	0.20	1	894.0	3.0	Etchback at junction, nonuniform layer.
0040	1.5	0.6	0.091	889	3	10	0.300	2	0.20	1	894.5	5.5	Etchback reduced; better coverage by grown layer.
0042	1.5	0.6	0.0856	887	3	10	0.300	2	0.20	1	894.0	7.0	Etchback not visible. Good uniform layer. Surface scratches.
0043	1.5	0.6	0.113	886.5	6.5	30	0.325	7	0.35	1	893.5	7.0	Same as above. Note change in growth rate. Surface scratches

[a]Besides the crushed GaAs added as specified, the melt was allowed to stay in contact with a thin wafer of GaAs during the saturation cycle.

[b]T_{ss}, °C, supersaturation temperature. After saturation at this temperature, the melt was allowed to cool down to the saturation temperature before the substrate was contacted to the melt.

[c]T_{sat} = Saturation temperature.

[d]ΔT = Cooling range of temperature.

[e]t_{min} = Cooling time.

[f]d = Thickness.

T983

30

M98II   2544 - II
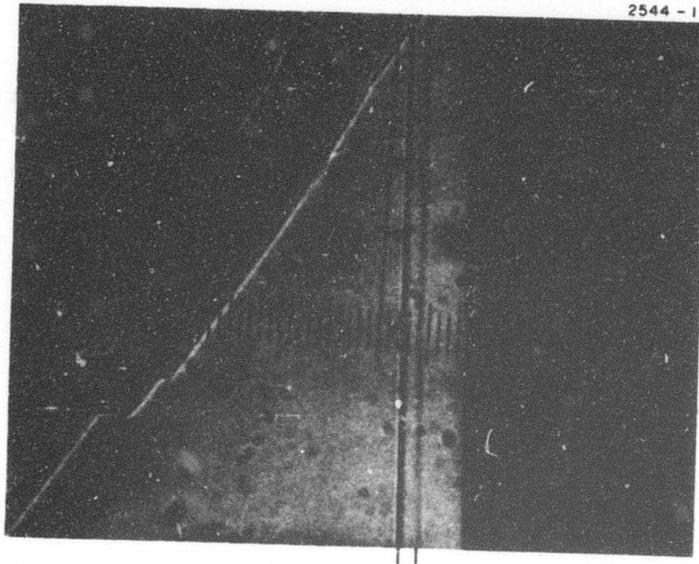
J₁ J₂   J₁ J₂ = REGROWTH REGION

Fig. 7.
Sample 0040.   GaAs with $Ga_{0.95}Al_{0.05}As$ epi-
layer. J_1J_2 shows the regrowth region close
to the junction.   Scale: 2 μm/div.
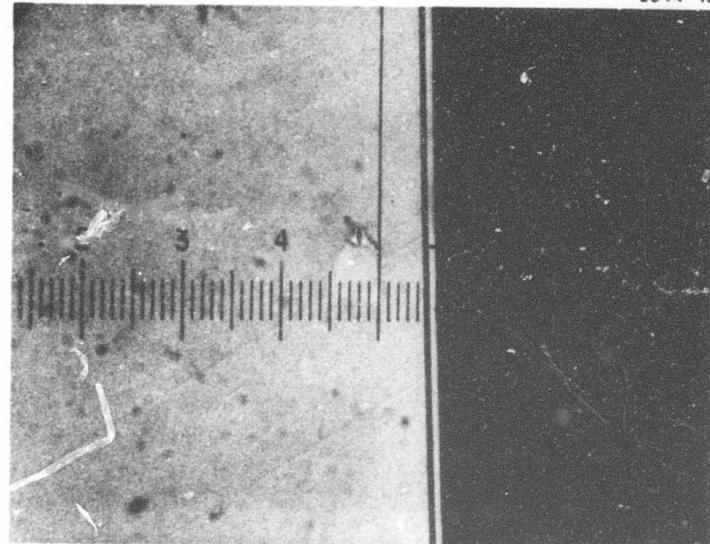
Fig. 8.
Sample 0042. $Ga_{0.95}Al_{0.05}As$ epilayer on
GaAs. No regrowth region observed.
cf. 0040. Scale: 2 μm/div.
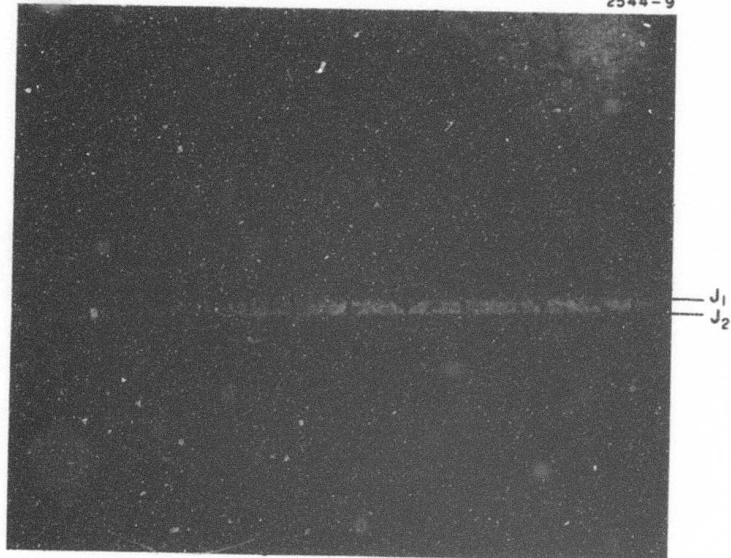
Fig. 9.
Ga$_{0.95}$Al$_{0.05}$As layer on GaAs. Note the
regrowth region $J_1 J_2$. Scale: 2.3 μm/div.
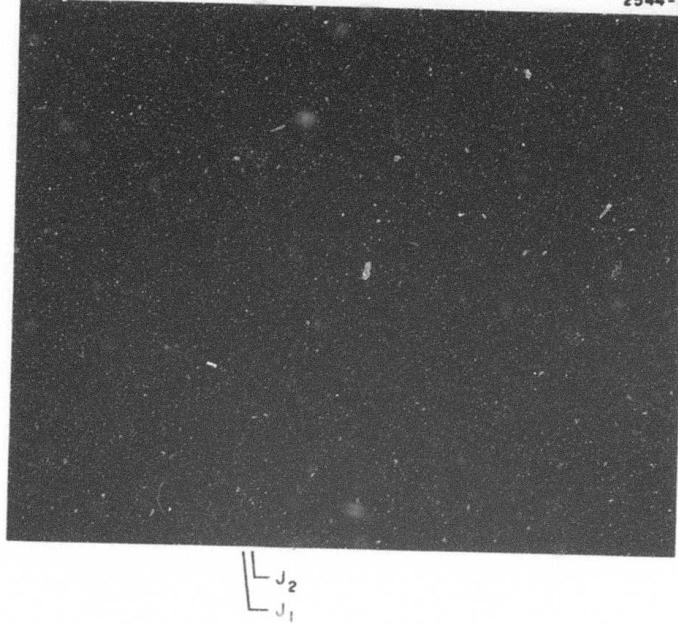
Fig. 10.
$Ga_{0.95}Al_{0.05}As$ layer on GaAs. Note increased thickness of epifilm, but same regrowth region J_1J_2. Scale: 2.3 μm/div.
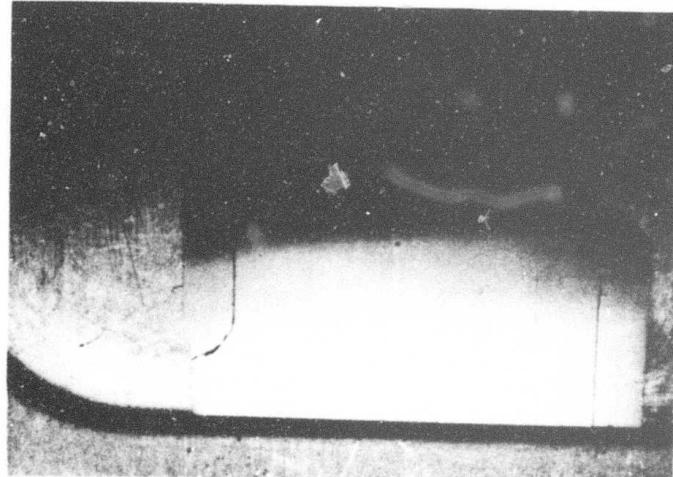
Fig. 11.
$Ga_{0.95}Al_{0.05}As$ layer on GaAs. Sample of a good layer. Note lines running parallel to cleavage lines at right and left end.

34

in the grown layer. The segregation coefficient being as high as 30 makes the solution poorer in aluminum, and hence the layer grown lower in aluminum concentration, as the growth progresses. However, this is offset to some extent by the increase in segregation coefficient as the temperature is reduced during the growth period. At any starting temperature, the final aluminum concentration profile in the epitaxial layer will be a reflection of these contradictory factors and the final result is heavily dependent on both the starting temperature and the growth cycle. It can be seen also from the argument that the thickness of the layer to be grown will have an important bearing on the starting temperature and the cycle to be chosen. Because of these considerations the limited melt epi is best used where thin layers are required and the infinite melt method described below has significant advantages when thicker layers of variable aluminum concentration have to be grown.

C.   Infinite Melt Liquid Epitaxy

The infinite melt technique offers many important advantages to the growth of semiconducting films, in general, and some specific advantages to the growth of $Ga_{1-x}Al_xAs$ films in particular. Since a large melt or saturated solution of GaAs in Ga is the source, the layer growth can be carried out in a stable matrix with very uniform conditions of temperature and concentration, the two prime parameters for good crystal growth. Again, since aluminum has a very high segregation coefficient, a uniform layer of $Ga_{1-x}Al_xAs$ can be grown easily from a large source so that the growth front concentration of the ambient liquid stays close to invariant during epitaxy. Hughes Research Laboratories has extensive experience in growing GaAs by infinite melt epitaxy, and therefore, is capable of evaluating the technique for the integrated optics application.

35

The major disadvantage to the large melt approach arises from the high reactivity of the aluminum. In the slide-bar approach this difficulty is avoided for two reasons inherent to the technique.

1. A small melt is used only in one experiment and then discarded. Therefore, the melt is exposed to air only once at the beginning of each experiment.

2. The substrate is slid under the melt and hence is not exposed to any reactive films that may be at the surface of the saturated melt. While this is helpful, it is well to remember that in the wiping operation, which is part of this process, any significant amount of surface crystallites or particles can lead to mechanical damage of the grown surfaces.

Thus, under controlled conditions the two points made here make the slide-bar limited-melt approach attractive. Its major advantage, of course, is its ability to make multiple films in one experiment by having more than one melt slide over the substrate in a series fashion. For some very small devices where feasibility and the determination of parameters for research are prime considerations, this is indeed a practical approach for obtaining rapid results. However, where large areas of perfect epitaxy are necessary, as in the case of waveguides, the infinite melt has the ability to provide large-area layers. The advantage of this approach can be appreciated further, when we think ahead to the next generation of device needs, where these waveguides have to be integrated with other structures to form integrated optics components and circuits.

With these goals in mind, we have proceeded with the growth of large-area $Ga_{1-x}Al_xAs$ films by the infinite melt technique. In most applications GaAs layers are grown from a melt contained in a quartz crucible heated to about 850°C.

36

Such layers have been grown in many laboratories. Generally, the layers grown from the undoped melt are p-type with silicon as the major impurity. In our experiments, we have been able to grow layers with p-type carrier concentration less than $10^{15}/cm^3$ routinely. However, when we added aluminum to the melt it was soon evident that a quartz crucible is not suitable, since it reacts with the aluminum at a rapid rate (see Table V, Q1 and Q2). We were forced, therefore, to look for alternative materials for crucibles.

One of the simplest of several alternatives is aluminum oxide. High purity aluminum oxide crucibles now are available for semiconductor use. Several of these have been purchased and we are conducting an extensive series of experiments to evaluate them for the growth of gallium arsenide epitaxial films.

The initial results have been very gratifying. Layers of $Ga_{1-x}Al_xAs$ have been grown and their electrical properties and chemical composition have been determined. It was evident from initial experiments that we had to provide for a more sophisticated gas handling and processing system for the crystal growth chambers to eliminate oxidation of the melt due to the addition of the aluminum. We have such a system being modified for $Ga_{1-x}Al_xAs$ crystal growth. A photograph of the system is shown in Fig. 12. It has a special sample entry chamber which can be independently evacuated and flushed with argon and, subsequently, with high purity hydrogen. Any sample that has to be introduced into the growth chamber must be introduced through this chamber. This eliminates all possibility of contamination of the melt during the long series of runs required to produce a number of samples. As the source melt itself is maintained in a constant flow of ultra-high-purity hydrogen at all times, it remains free of oxide and other contaminants which may be

TABLE V

Growth of $Ga_{1-x}Al_xAs$ by Infinite Melt Epitaxy

Melt Number	Composition Weight in Grams	Growth Temperature °C	Epi Layer			
			Al Concentration Atomic Percent[b]	Layer Thickness, μm	Carrier Concentration, cm^{-3}	Mobility, $cm^2/V\text{-}sec$
Q_1	Ga = 80 GaAs = 7.5 Al = 0.048	829	0	28	2×10^{17} (p-type)	140
Q_2[a]	Ga = 80 GaAs = 7.5 Al = 0.048	860	0	29	4.5×10^{17} (p-type)	93
A_1	Ga = 100 GaAs = 10	840	0	50	4×10^{16} (n-type)	2950
A_2	Ga = 100 GaAs = 10 Al = 0.1	860	5	10	1.5×10^{17} (n-type)	1370
A_3	Ga = 100 GaAs = 10 Al = 0.3	875	14		Data Incomplete	
A_4	Ga = 100 GaAs = 10 Al = 0.5	876	24	23		

[a]Q_2 is the same melt as Q_1, but the layer was grown after the melt stayed at temperature for 48 hours longer. Both were grown using quartz crucibles.

[b]Concentration determined by electron microprobe. The values in x units would be twice the atomic percent.

T984

38

M9252
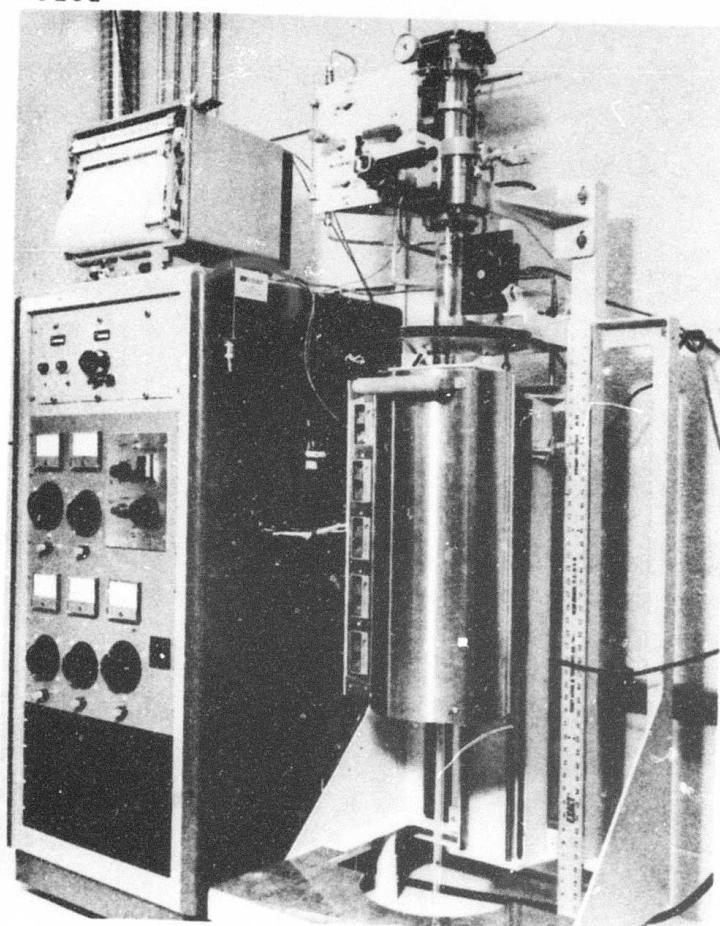
Fig. 12. Reactor for liquid epitaxy.

introduced inadvertently during the entry of the substrate into the chamber. We have observed that over a period of time the melt gets cleaner progressively and then stays extremely clean throughout a long series of experiments.

The growth system is equipped with an Azar recorder-controller backed up by a very sensitive proportional-type controller that allows accurate measurement and control of temperature in a five-zone furnace. We have also perfected a programmer that can smoothly vary the rate of temperature change as a function of time. The combination allows us to study the epitaxial layer growth as a function of the temperature cycle and hence to establish an optimum program for fully reproducible epitaxial layer growth.

Data gathered from the slide-bar assembly experiments were used as a starting point to calculate the concentration of aluminum and gallium arsenide necessary to obtain layers with different compositions of grown layer. Table V gives the growth parameters and characterization results for several melts and the properties of crystals grown from them. The first two, Q_1 and Q_2, refer to layers grown from quartz. It is interesting to note that both these layers show no trace of aluminum in the grown layer. Layer A_1 gives the characteristics of a layer grown from the undoped melt in the aluminum oxide crucible. Since it was a new crucible and an early experiment in a series with aluminum oxide crucibles, the carrier concentration is considerably higher than the method is capable of giving. It is interesting, however, that the layer is well behaved as shown by the mobility. Note that aluminum is absent from the epitaxial layer, even though aluminum oxide crucible was used.

Layers A_2 through A_4 were grown with the addition of aluminum. The values of Al concentration obtained by the electron microprobe need to be corrected to take into account absorption caused by Ga and Al. We are perfecting a computer program which will enable us to do this routinely on our samples. The data given here, however, indicate that the method is dependable and can be used controllably to produce $Ga_{1-x}Al_xAs$ layers with predictable aluminum concentrations.

The surface of the grown layers is smooth and uniform, and the grown junction is free from imperfections (see Figs. 13 and 14). More detailed measurements with the electron microprobe presently are being made, and these will be confirmed by independent measurements using photoluminescence.

Several additional factors, which influence the quality of the epitaxial layer and the aluminum concentration profile in it, will be investigated in the next quarter. These include the starting temperature, the rate of cooling, and the temperature range of the cooling cycle that is optimum for a specific aluminum concentration in the layer. The aluminum concentration profile will be determined accurately by polishing the epitaxial layer on a bevel.

M9810
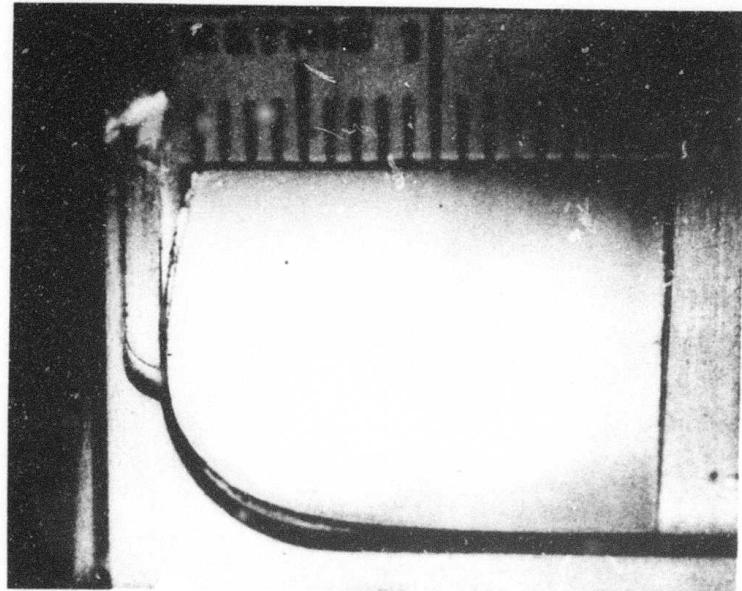
Fig. 13.
$Ga_{0.5}Al_{0.5}As$ layer grown by the infinite
melt method. Layer thickness 65 μm. Note
the smooth, featureless surface over the
entire area.

M 9812   2544-12
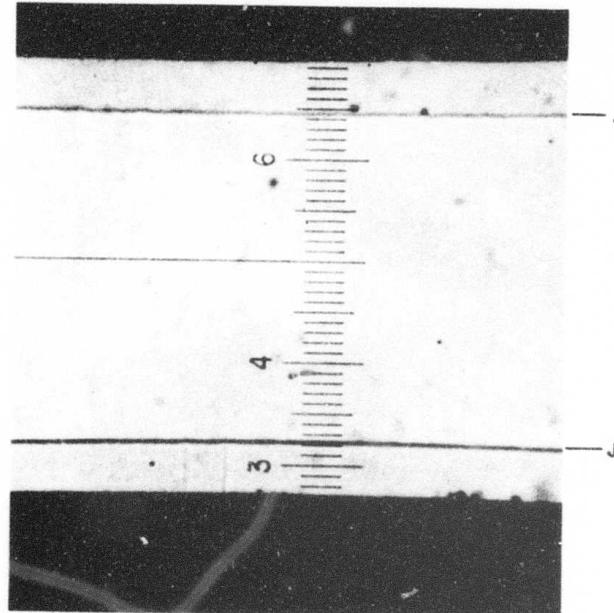
J – JUNCTION
A & B SIDES ARE
BOTH SHOWN

Fig. 14.
$Ga_{0.5}Al_{0.5}As$ grown by infinite melt method.
Thickness 65 µm. The two epitaxial layers on
the crystals are clearly brought out to show
the uniformity of the layers.

IV. EPITAXIAL FILM CHARACTERIZATION

A. Physical and Chemical Evaluation

Reference has been made in the preceding section to evaluation and characterization of layers grown during the program. Hall measurements have been made on several samples to determine carrier concentration and mobility (see Table V in Section III-C), and electron microprobe measurements have been used to determine the aluminum concentration and the concentration profile in several samples grown by the infinite melt and limited melt techniques.

One of the points worth noting is that the layer thickness measured by the optical microscope on a cleaved, etched cross section of the grown layer checks closely with that measured by the scanning electron microscope. The aluminum concentration measured using the electron microprobe shows abrupt variation at the junction and a gradation across the layer (see Figs. 15 through 19). Figures 15(b) through 19(b) also show the variation in aluminum as the melt concentration changes. For each sample the Al K_α scan indicates no noticeable variation in uniformity. Accurate quantitative measurements using the electron microprobe must await a detailed computer program that is being perfected. This program is necessary since the aluminum peak, because of its close proximity to the gallium and arsenic peaks and aluminum's small atomic number, needs to be corrected for absorption effects. Additional correction is necessary since the position of the aluminum peak calls for operation of the microprobe at as low a potential as possible to avoid heavy backscattering. The program presently is being refined to enable us to measure the aluminum concentration quantitatively at several Al levels.

45
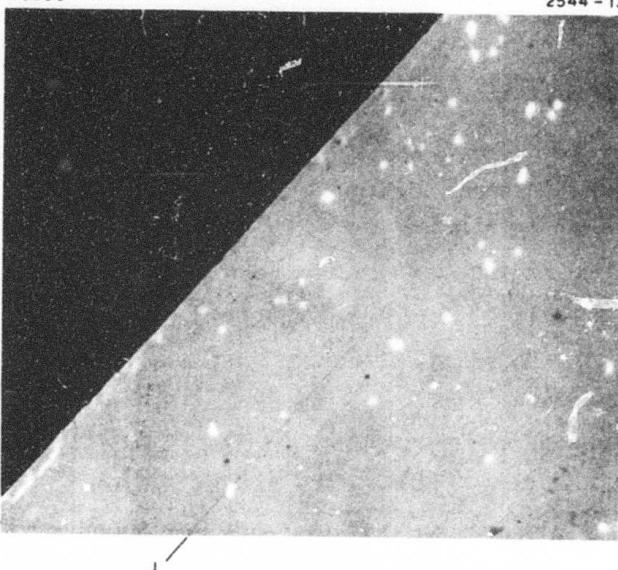
Fig. 15(a).
SEM photograph of
cleaved cross sec-
tion of Q_2 (Table
IV). Magnification
500x.

Fig. 15(b).
AlK_α scan of Q_2
(same region as
15(a)). Magnifi-
cation 500x.

J = JUNCTION
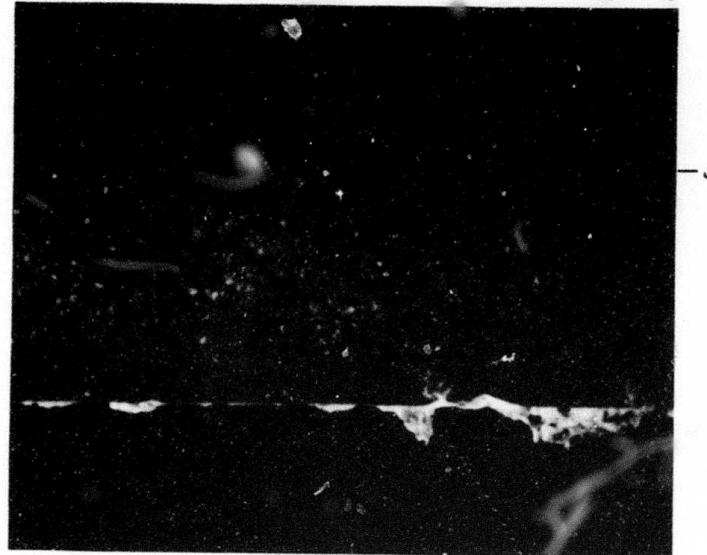
Fig. 16(a). SEM photograph of cleaved cross section of A_1 (Table IV). Magnification 500x.
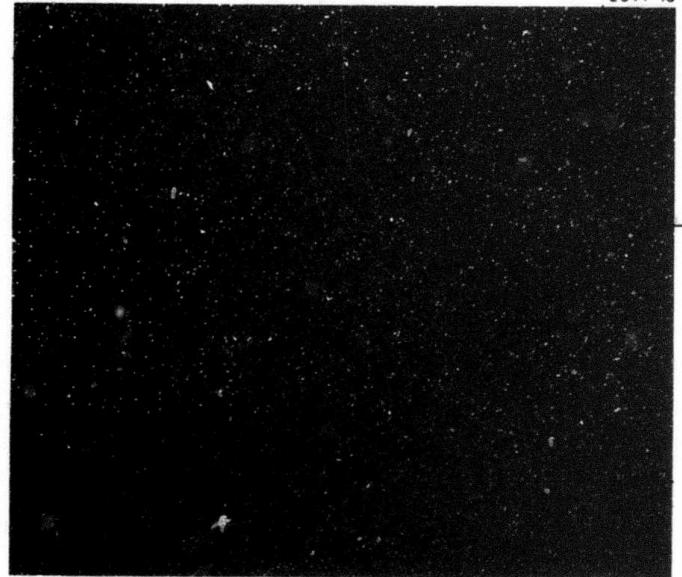
Fig. 16(b). AlK_α scan of A_1 (same region as 16(a)). Magnification 500x.
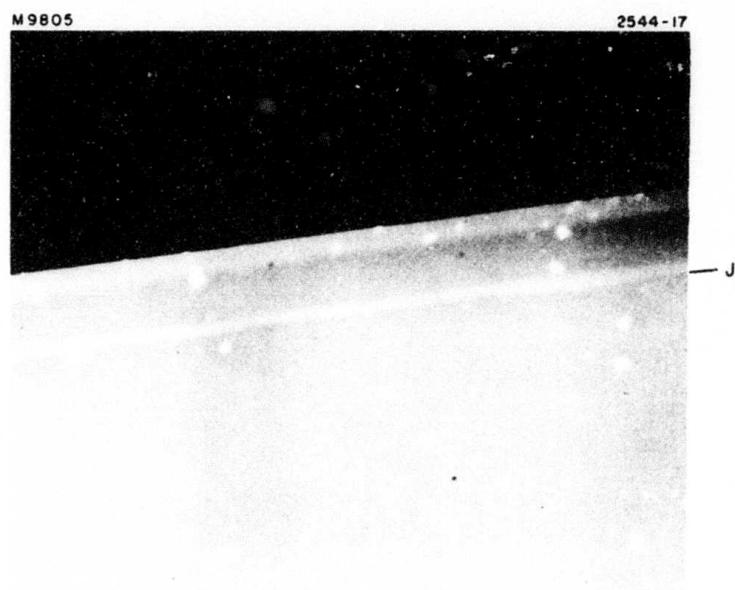
Fig. 17(a).
SEM photograph
of cleaved cross
section of A_2
(Table IV).
Magnification
500x.

Fig. 17(b).
AlK_α (same
region as 17(a)).
Magnification
500>.

M9807
2544-19

Fig. 18(a).
SEM photograph
of cleaved
cross section
of A_4. Magni-
fication 500x.

M9802
2544-20
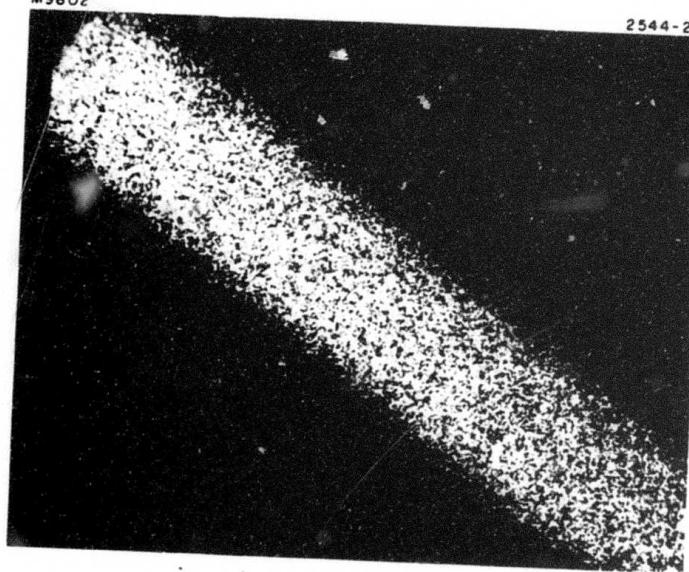
J = FUNCTION

Fig. 18(b).
AlK_α scan of A_4
(same region as
18(a)). Magni-
fication 500x.

49

O-2544-27

J
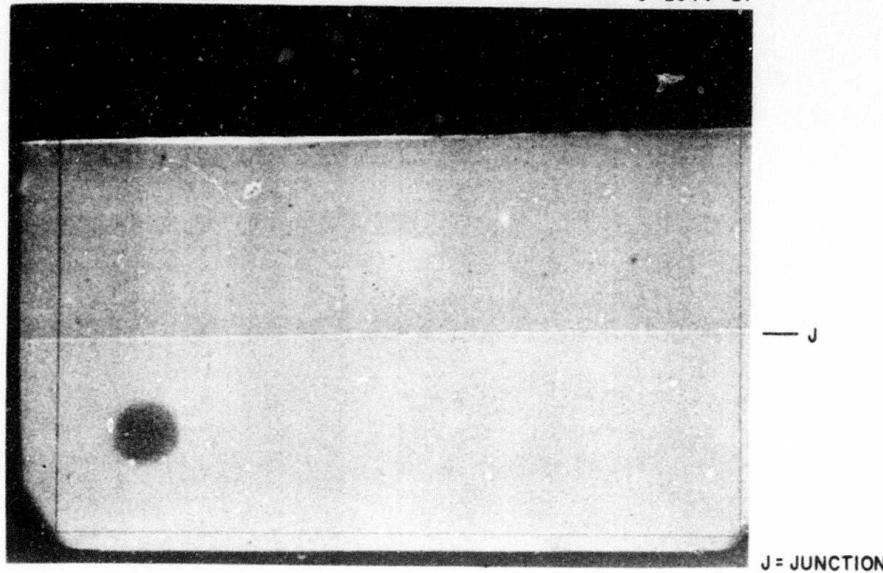
J = JUNCTION

Fig. 19(a). SEM photograph of cleaved cross section
of A_4 (Table IV). Magnification 500x.

O-2544-28

J
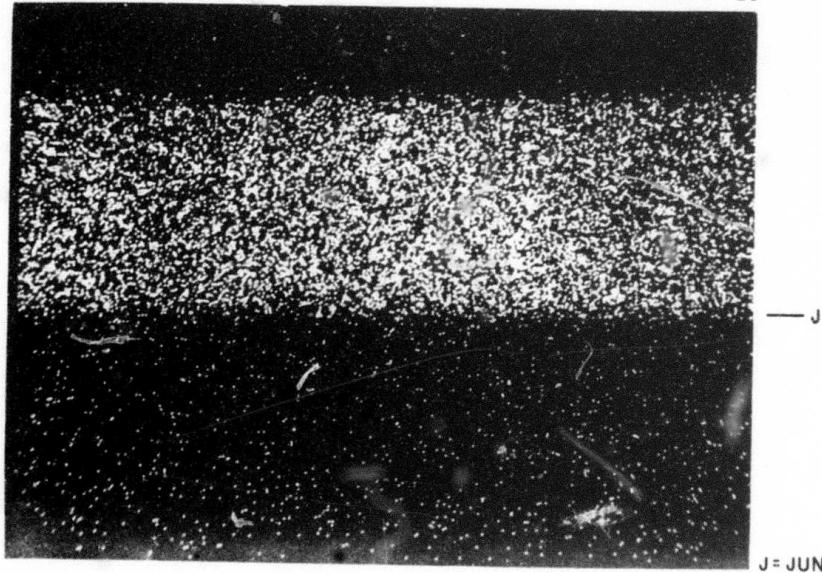
J = JUNCTION

Fig. 19(b). AlK_α scan of A_4. (Same region as 19(a)).
Magnification 500x.

50

We also have obtained electron microprobe profiles of the cleaved cross section of sample A_4 listed in Table V. This is shown in Fig. 20. As can be seen from this figure, there is only a small gradient of the Al concentration across the epitaxial layer. A comparison between the layer grown in the infinite melt and a previous one from the limited melt approach illustrates the influence of the segragation coefficient, highlighting the difference between the two techniques. The dramatic difference between the two methods in providing thick uniform layers is obvious from Fig. 21. In Fig. 21 the Al/Al_j refers to the ratio of aluminum concentration at a certain distance from the junction to that at the junction itself. It can be seen that the infinite melt method gives almost the same variation in concentration in 27 μm as the slidebar method gives in 4 μm. Considering that the infinite melt growth took place at 875°C and the slidebar method at 896°C, the variation for the infinite melt at comparable temperature should be even less since the segregation coefficient is lower for the higher temperature of growth. We have the capability of reducing the concentration variation even further by two different approaches: (1) increase the melt volume and (2) increase the temperature at which growth is started. Both these will be used in combination to grow epitaxial layers of $Ga_{1-x}As_xAs$ of varying aluminum content. We also shall be studying the aluminum profile in greater detail by using beveled samples for microprobe analysis.

B.   Optical Waveguiding Evaluation

An attempt has been made to measure the loss of a GaAs epitaxial waveguide on a 4% Al concentration $Ga_{1-x}Al_xAs$ substrate. The GaAs layer was grown by vapor phase epitaxy and was approximately 5 μm thick. Coupling into and out of the

51
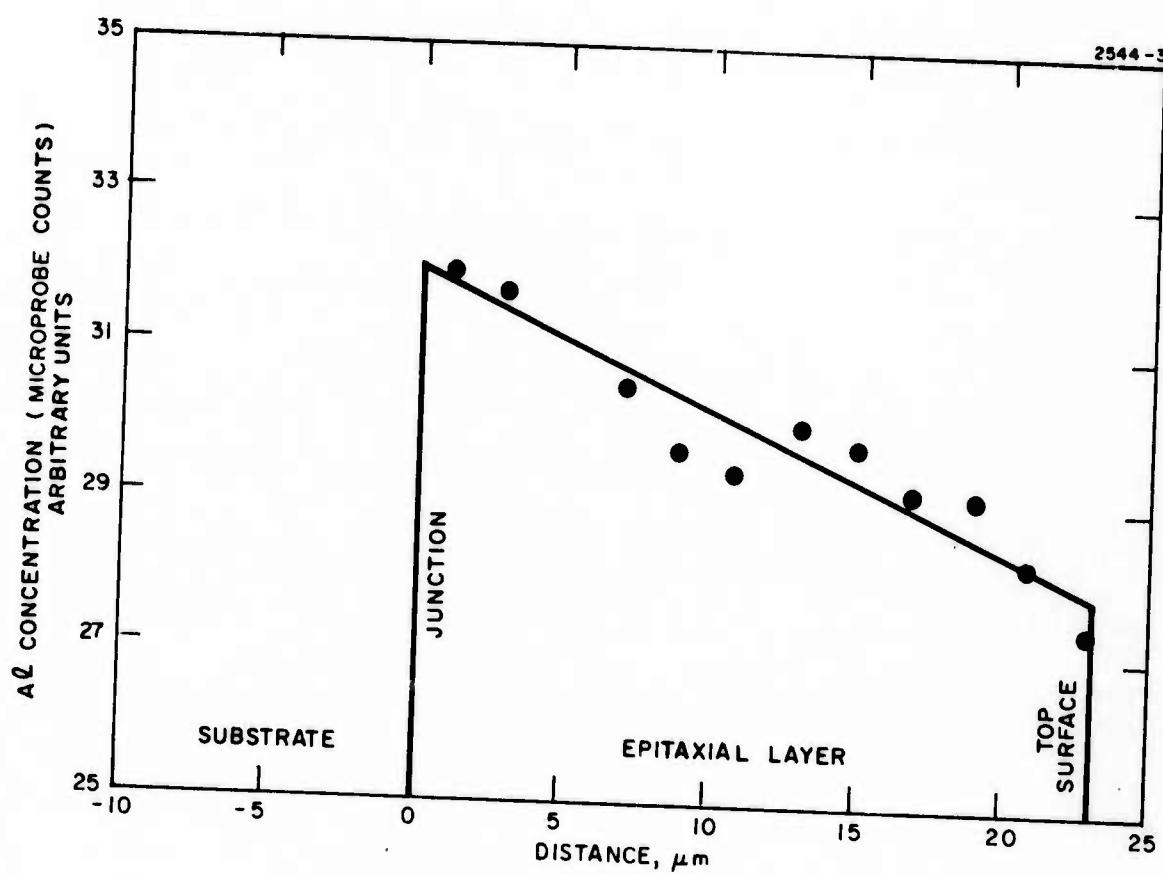
Fig. 20. Infinite Melt epitaxy: aluminum concentration pro-
file of cleaved cross section. Sample A_4. Scat-
ter in the points partly due to the cleaved inter-
face irregularity as seen by the microprobe.

52
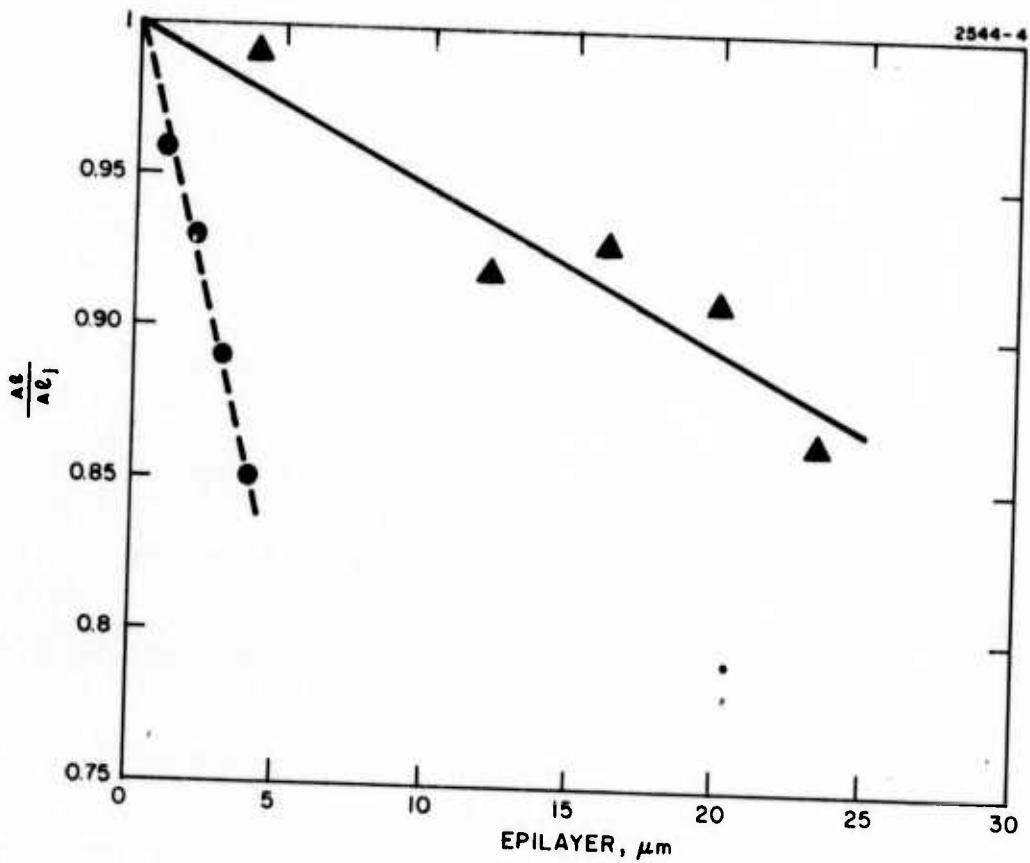
Fig. 21. Electron microprobe profile of $Ga_{1-x}Al_xAs$ layers grown by different methods.
– – – by slide bar (sample 0001).
——— by infinite melt (sample A_4).

$$\frac{Al}{Al_j} = \frac{\text{Concentration of aluminum at a point in layer}}{\text{Concentration of aluminum at growth interface}}$$

waveguide was achieved by direct focusing onto the cleaved edges. The intensity profile from the output face of the waveguide was recorded using a Ge photodetector. The radiation source is a He-Ne laser operated on the 1.15 μm transition. Samples of varying length were cleaved from a single wafer. If the attenuation loss per unit length is uniform, then a semilog scale plot of the relative output intensity versus length should yield a straight line whose slope is equal to the intensity absorption coefficient. The results obtained for five lengths measured are shown plotted on a log scale in Fig. 22. For a fixed length the different data points are the result of propagation through a different portion of the slab guide. As can be seen, the data points do not lie on a straight line. High magnification photographs (shown in Fig. 23) of the cleaved surfaces of the various samples indicated that the surface quality was not optimum, a fact which undoubtedly resulted in varying input-output coupling losses. The straight line shown in Fig. 22 corresponds to a 2.2 cm^{-1} absorption coefficient.

Optical waveguiding has been observed through approximately 2 mm of $Ga_{0.98}Al_{0.02}As$ liquid phase epitaxial waveguide on a substrate of $Ga_{0.95}Al_{0.05}As$. The guide thickness is 2 to 3 μm. The relative output intensity was weak compared with the vapor phase GaAs guiding structure described previously. It is felt that thus is attributable to poor surface quality of the epilayer.
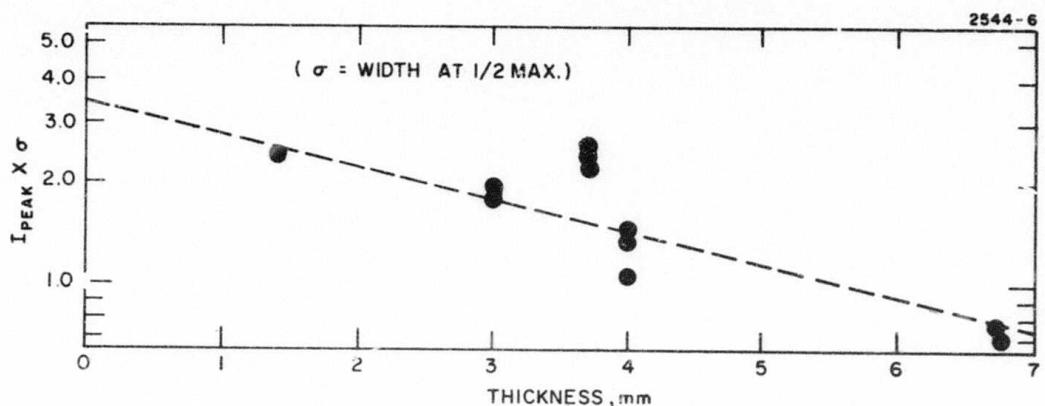
Fig. 22.   Loss measurement data on GaAs epitaxial waveguide
on a 4% Al concentration $Ga_{1-x}Al_xAs$ substrate.
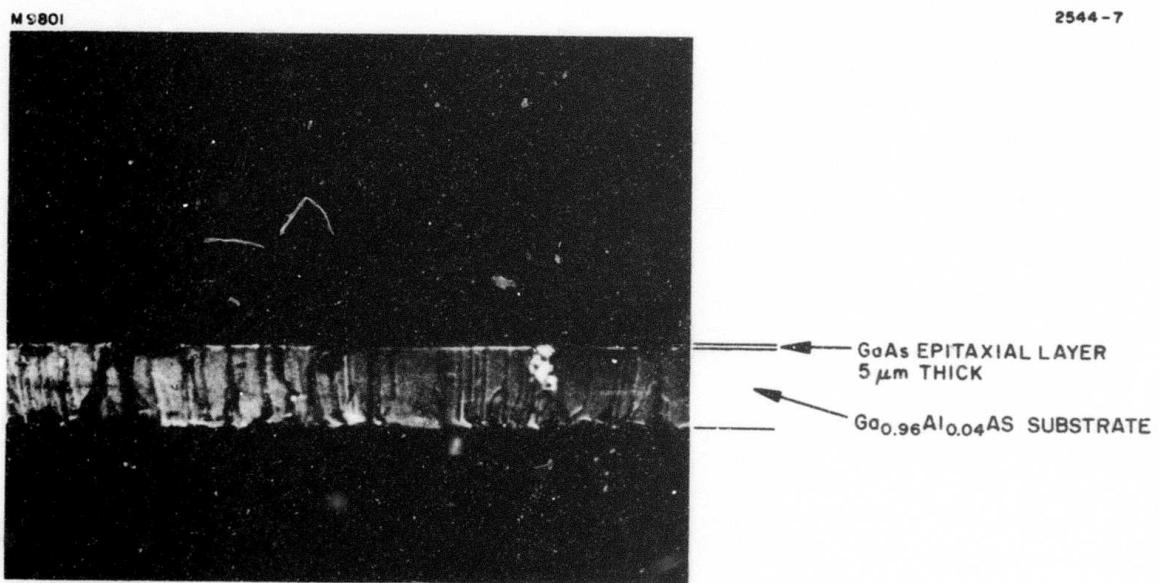
Fig. 23.   Example of a cleaved edge of a GaAs epitaxial
waveguide on a 4% Al concentration $Ga_{1-x}Al_xAs$
substrate.

V. DEVICE ELEMENTS

During this reporting period we have begun considering some of the device elements for which GaAs and $Ga_{1-x}Al_xAs$ are particularly suitable, with the aim of establishing the relationship between device requirements and material and structure characteristics. In this area some of the company-supported efforts in specific device areas are proving to be helpful.

A. Integrated Optics Components

1. Waveguide Bends and Couplers

Waveguide bends are clearly a necessary part of integrated optical circuitry. An estimate of the radiation loss for a bent waveguide with a radius of curvature R can be obtained from the analysis of Marcatili.[4] As an example, consider an infinitely high slab guide of thickness "a" and refractive index n_x imbedded in a medium of refractive index n_y so that $n_y = n_x(1-\Delta)$ with $\Delta<<1$. Following example two of Ref. 2, the guide dimensions required for a total curvature radiation loss $\alpha R = 0.01$ nepers $= 0.087$ dB are listed in Table VI. It is assumed that the width a is the maximum compatible with single mode guidance in the infinitely high slab, that is

$$2\left(\frac{a}{\lambda_0}\right)\left(n_x^2 - n_y^2\right)^{1/2} = 1$$

Assuming that $n_x = 3.569$ (GaAs) the results obtained are listed in Table VI.

---

[4] E.A.J. Marcatili, Bell Syst. Tech. J. 48, 2103 (1969).

57

Preceding page blank

TABLE VI

Guide Characteristics Computed for Total Bend Loss of $\alpha R = 0.087$ dB

Δ	$y - x$	$\dfrac{a}{\lambda}$	$\dfrac{R}{\lambda}$
0.10	0.3	0.32	12
0.01	0.05	0.99	376
0.001	0.005	3.13	11,900

As can be observed from the numbers in Table VI, a 5% Al concentration difference is theoretically sufficient to ensure reasonable radii of curvature. This needs to be experimentally verified.

Coupling of energy from one channel optical waveguide into an adjacent optical waveguide recently has been demonstrated.[5] The channel waveguides were formed by proton implanting GaAs. It was shown that efficient coupling between the excited channel and adjacent channels is possible. This demonstration of efficient coupling along with the fact that guides in $Ga_{1-x}Al_xAs$ have reasonable radius of curvature losses for Al concentration differences on the order of 5% make couplers of the type sketched in Fig. 24 feasible. Here, the relationship between the geometry of the device and the Al concentrations in the various layers is even more critical than for ordinary guides and bends.

2. Distributed Feedback Injection Laser

Thin film waveguides fabricated in the $Ga_{1-x}Al_xAs$ material system offer the attractive possibility of providing

[5] S. Somekh, E. Garmire, A. Yariv, H.L. Garvin, and R.G. Hunsperger, Appl. Phys. Lett. 22, 46 (1973).

2360-2
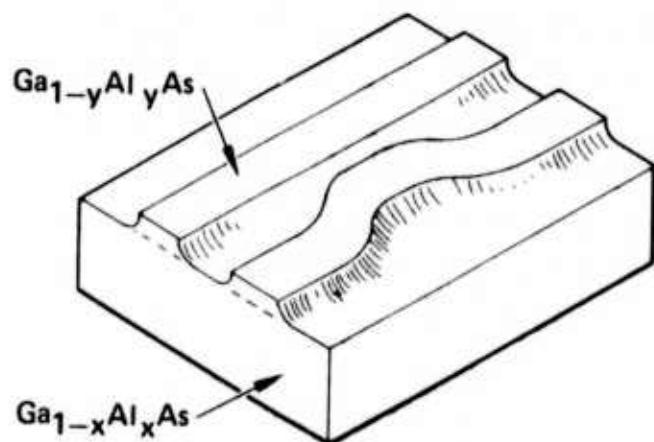
(a) RIDGED GUIDE COUPLER

2360-3

INDEX FILLING MATERIAL TO
INCREASE COUPLING COEFFICIENT

$Ga_{1-x}Al_xAs$

$Ga_{1-y}Al_yAs$

$Ga_{1-y}Al_yAs$
ORIGINAL EPITAXIAL LAYER
DOPED WITH ADDITIONAL
ALUMINUM TO FORM LATERAL
INDEX DISCONTINUITY
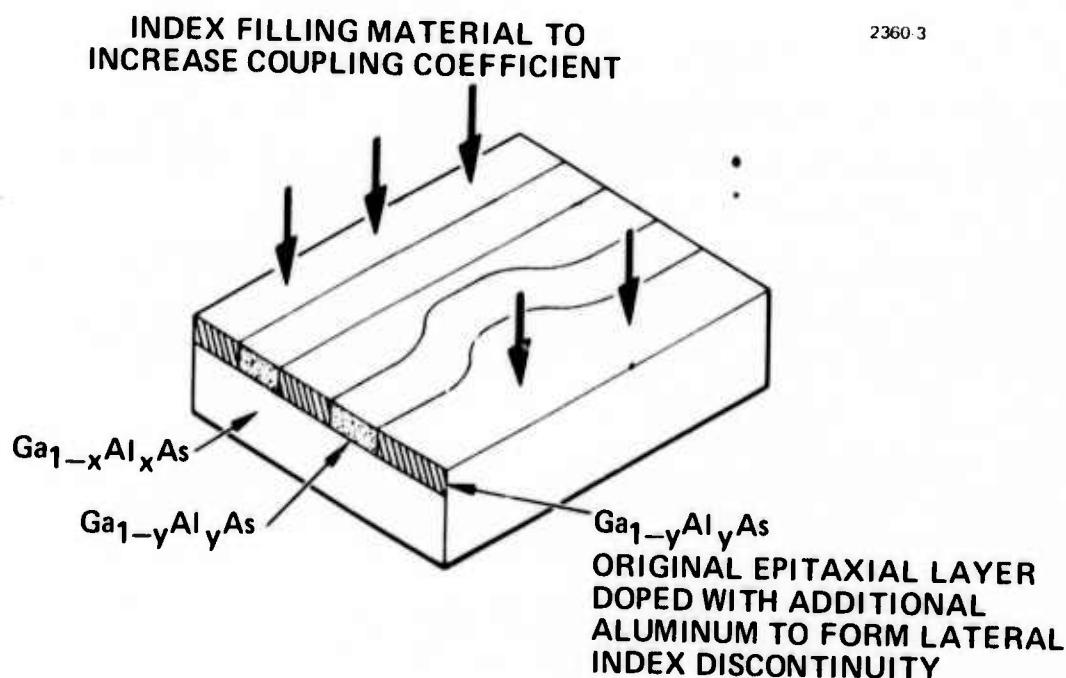
(b) PLANAR GUIDE COUPLER

Fig. 24. Narrow optical waveguide couplers.

59

an electrically pumped thin film source. A sketch illustrating what the future may hold with regard to thin film sources is shown in Fig. 25. The active region consists of a p-n junction in a GaAs layer. Feedback for lasing action is provided by the periodically corrugated surface. The first order Bragg feedback condition requires a corrugation period of 1200 $\overset{o}{A}$. To prevent the radiation from being absorbed in the waveguide coupled to the laser, the Al concentration in that region must be sufficient to shift the bandgap of the $Ga_{1-y}Al_yAs$ guide away from that of GaAs. The major problems in building a distributed feedback injection laser are the machinability of GaAs to required tolerances and the development of techniques for fabricating structures with composition discontinuities along the epitaxial layer.

3. Integrated Detectors

Bombardment of GaAs with high energy protons can be used advantageously in the fabrication of optical detectors. Proton bombardment causes an absorption edge shift to energy low enough to permit detection of photons which can be guided with little absorption in waveguides formed in the GaAs by any of the usual methods.

Under company funding we have fabricated two types of detectors using proton bombardment. One of these is of the type which has a transparent surface barrier to admit the light to the active volume. The barrier was fabricated by evaporating a 130 $\overset{o}{A}$ thick gold film. The second type of device is an integrated waveguide-detector combination with evaporated aluminum surface barrier. Preliminary measurements of device characteristics such as Schottky barrier reverse breakdown voltage, photocurrent, avalanche multiplication photoresponse, and time response have been performed. These characteristics are related to such material parameters

60
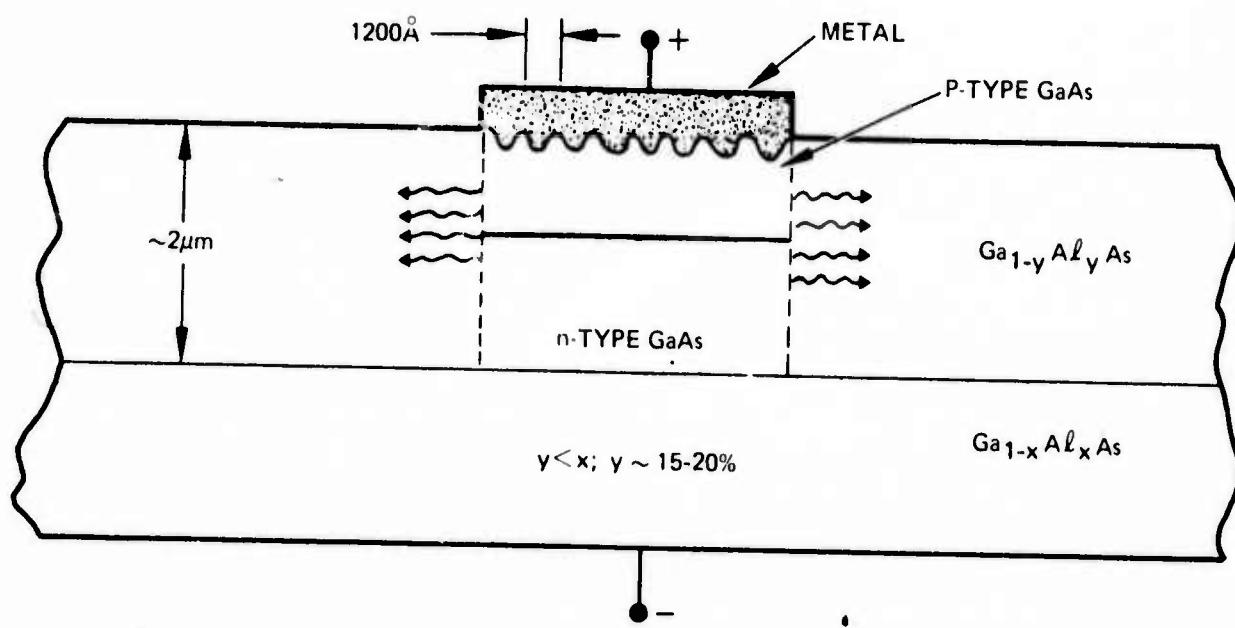
Fig. 25. Concept for a thin film integrated source.

as carrier concentration and mobility, density and distribution of defects or contaminant atoms producing deep level traps, and epitaxial layer thickness uniformity. Therefore, evaluation of these properties and determination of the effect of the growth techniques on these properties is essential.

4.   Thin Film Modulator

In addition to sources, detectors, channel waveguides, and directional couplers, a complete integrated circuit will require a means of modulation. If the source is an injection, laser modulation may be achieved by direct modulation of the source itself. Alternatively, the integrated optical circuit may possess a separate thin film modulator. If the electro-optic effect is used for the modulator one must properly select the layer-substrate index difference, guide thickness, and crystal orientation so that the application of an external voltage can force the guide in and out of cutoff. This produces an amplitude modulated signal at the output coupler. Since metal electrodes must be used to enable one to apply the electric field the material and structure properties affecting the Schottky barrier at the electrode, the depletion layer in the modulator film, and the amplitude of the optical field at the electrode (affecting losses) must be carefully considered.

5.   Periodic Optical Filter

As the state-of-the-art of integrated optics progresses, a need can be foreseen for optical filters compact enough to be compatible in integrated optical circuits. Periodically perturbed guides can be used as such filters. The filtering action of a periodic guide is based on the fact that frequencies near the Bragg regime where the wavelength fulfills the condition,

$$\Lambda = m \frac{\lambda}{2}, \ m = 1,2,3 \ldots$$

62

are rejected. Here Λ is the period and m represents integers. A detailed analysis of periodic filters is given in the following section.

B.   Analysis of Propagation Characteristics of Periodic Dielectric Waveguides

Periodic optical structures are expected to play an important role in integrated optics. Their applications include, (1) optical filters, (2) grating-air waveguide couplers, (3) directional coupling, and (4) distributed feedback lasers.

A basic understanding of the propagation characteristics of such waveguides is a prerequisite to their utilization. We have considered the problem from two points of view: (1) direct solution of Maxwell's equations, and (2) coupled mode formalism.

The first approach is important in understanding the general propagation and radiation behavior of the periodic waveguide. The second one is especially useful near the Bragg regime where the period Λ is some integral multiple of $\lambda/2$ where λ is the wavelength in the guide. It also leads to closed form expressions for some of the needed engineering parameters of the structure.

The periodic structure considered in our work is the corrugated dielectric waveguide.[6,7] Techniques for producing such corrugations using ion milling[8] have been developed to the point where gratings with $\Lambda = 0.11\mu$ have recently been fabricated.[9] The structure considered in this part of the analysis is shown in Fig. 26.

[6]K. Sakuda and A. Yariv, Optics Communications 8, 1 (1973).
[7]H. Stoll and A. Yariv, Optics Communications 8, 5 (1973).
[8]H.L. Garvin, E. Garmire, S. Somekh, H. Stoll, and A. Yariv, Appl. Optics 12, 455 (1973).
[9]H. Yen, et al., to be published in Optics Communications.

$$x = \frac{d}{2} - \Delta \cos\left(\frac{2\pi}{\Lambda} z\right)$$
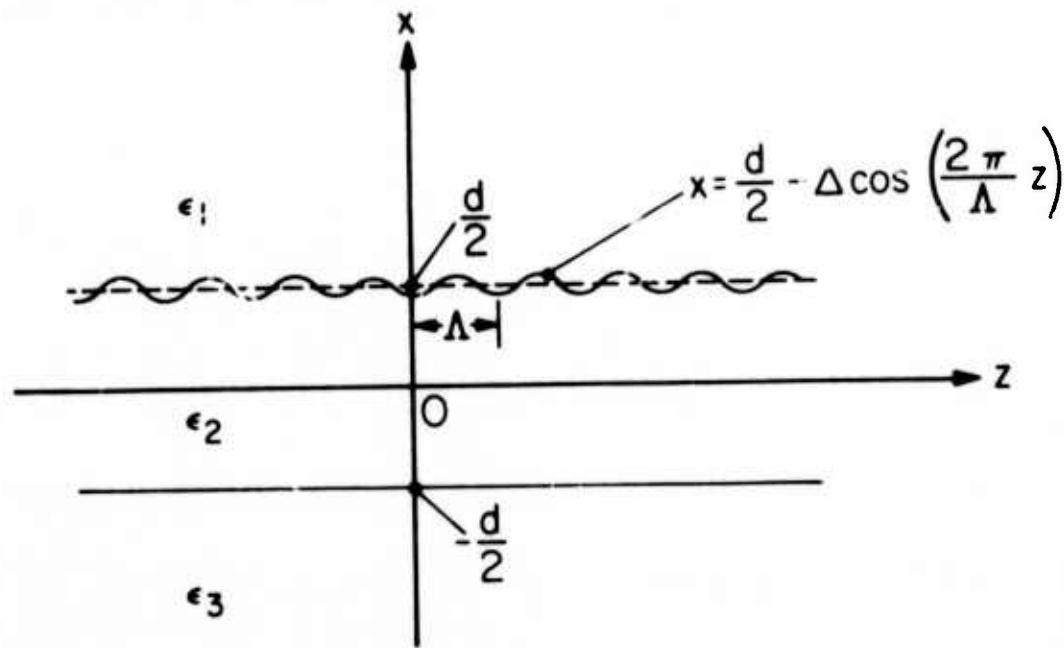
Fig. 26. Schematic of thin film dielectric waveguide with a sinusoidal corrugation on one side of a guide. Corrugation height 2Δ, waveguide thickness d, periodicity Λ.

The model consists of a three-layered waveguide with sinusoidal corrugation. We assume no variation in the y direction and consider the propagation of a TM mode. The modification necessary to obtain the behavior of a TE mode will be described below.

Assuming $\exp(-i\omega t)$ variation, we obtain from Maxwell's equations

$$\left(\nabla_t^2 + n_j^2 \, k_o^2\right) H_{yj} = 0 \quad , \tag{1}$$

$$E_j = (i/\omega\epsilon_j) \, \nabla_t \times (H_{yj}\hat{y}) \quad , \tag{2}$$

where $\nabla_t = \hat{x}\partial/\partial x + \hat{z}\partial/\partial z$, n_j is the index of refraction of layer j (j=1,2,3) and $k_o = \omega(\mu_o\epsilon_o)^{1/2}$. The propagating mode at ω has a Floquet form and is taken as

$$H_{y1,n} = \sum_{m=-\infty}^{\infty} A_{m,n} \, \exp(i\beta_{m,n}z) \, \exp(-\gamma_{m,n}x) \quad ,$$

$$x \geq d/2 - \Delta \, \cos(2\pi z/\Lambda) \quad ; \tag{3}$$

$$H_{y2,n} = \sum_{m=-\infty}^{\infty} \exp(i\beta_{m,n}z)$$

$$\times \left[B_{m,n} \, \exp(i\alpha_{m,n}x) + C_{m,n} \, \exp(-i\alpha_{m,n}x) \right] \quad ,$$

$$-d/2 \leq x \leq d/2 - \Delta \, \cos(2\pi z/\Lambda) \quad ; \tag{4}$$

$$H_{y3,n} = \sum_{m=-\infty}^{\infty} D_{m,n} \, \exp(i\beta_{m,n}z) \, \exp(\xi_{m,n}x) \quad ,$$

$$x \leq -d/2 \quad . \tag{5}$$

n refers to the mode index, while m denotes the mth space harmonic of the nth mode. The problem consists of solving for the space harmonic amplitudes and the propagation constants $\gamma_{m,n}$, $\alpha_{m,n}$, $\xi_{m,n}$, and $\beta_{m,n}$. The last four are related through the wave eq. (1) as

65

$$\gamma^2_{m,n} = \beta^2_{m,n} - n^2_1 k^2_0 \quad , \quad \alpha^2_{m,n} = n^2_2 k^2_0 - \beta^2_{m,n} \quad ,$$

$$\xi^2_{m,n} = \beta^2_{m,n} - n^2_3 k^2_0 \quad , \tag{6}$$

where

$$\beta_{m,n} = \beta_n + 2m\pi/L \quad . \tag{7}$$

Note that in view of eq. (7) we need only solve for $-\pi/L < \beta_n < \pi/L$ and the rest of the dispersion ($\omega-\beta$) diagram can be obtained from eq. (7).

Applying the continuity conditions to E_t and H_t at the two interfaces leads to an infinite set of homogeneous algebraic equations for the coefficients $A_{m,n}$, $B_{m,n}$, $D_{m,n}$. Truncating the number of terms in the resulting determinantal equation and solving it numerically on a computer leads to the dispersion relations. These are drawn in Figs. 27, 28, and 29 for the parameters:

Corrugation height: $2\Delta = 0.3$ μm
Thickness of waveguide: $d = 3$ μm
Periodicity: Λ arbitrary
$n_2 = 3.6$
$n_3 = 3.4$

Notice the existence near $\beta\Lambda = \pi$ of a forbidden frequency regime. In this regime which is magnified in detail in Fig. 29, the propagation constants are complex. This is a result of Bragg scattering between the forward ($\beta\Lambda = \pi$) and the backward ($\beta\Lambda = -\pi$) traveling waves which becomes resonant when $2\pi/\Lambda = 2\beta$. This is the region which is most useful in distributed feedback lasers[9] and in optical filtering. This region can be studied by assuming that the optical

---

[9]Ibid.
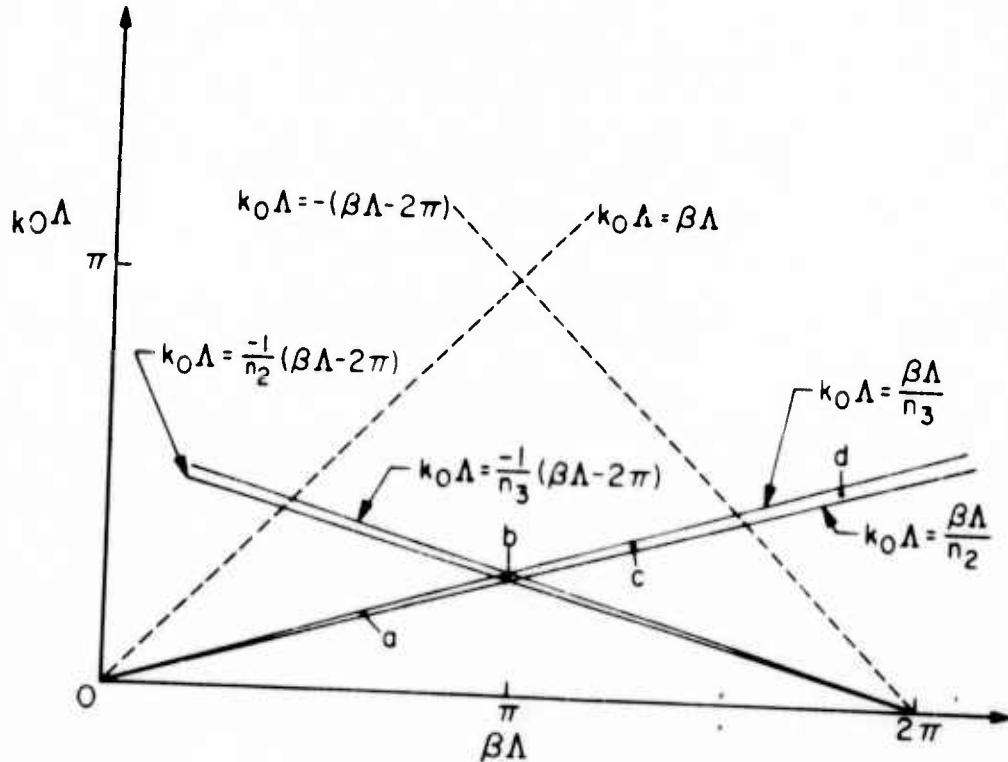
Fig. 27. Asymptotic lines of dispersion diagram (solid lines). If dispersion curve lies in regions a and b, the mode is confined in a guide. In region c the guided modes couple to a substrate leaky mode. In region d the guided modes couple to both air and substrate leaky modes.
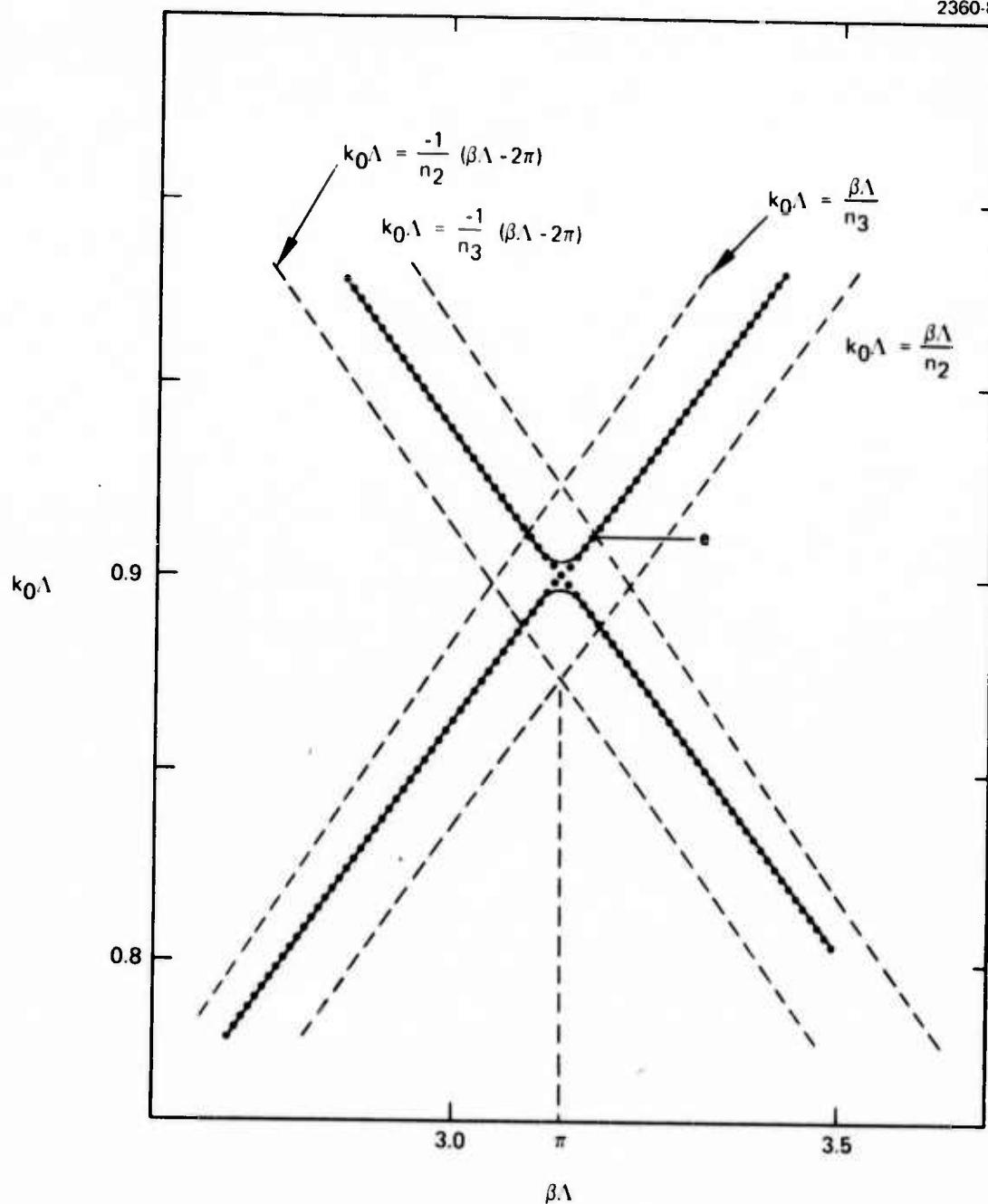
Fig. 28. Dispersion diagrams for a corrugated and an un-corrugated waveguide. Solid lines show the dispersion diagram for a sinusoidally corrugated waveguide. Dotted lines show the dispersion diagram for an uncorrugated waveguide (TM mode).

68
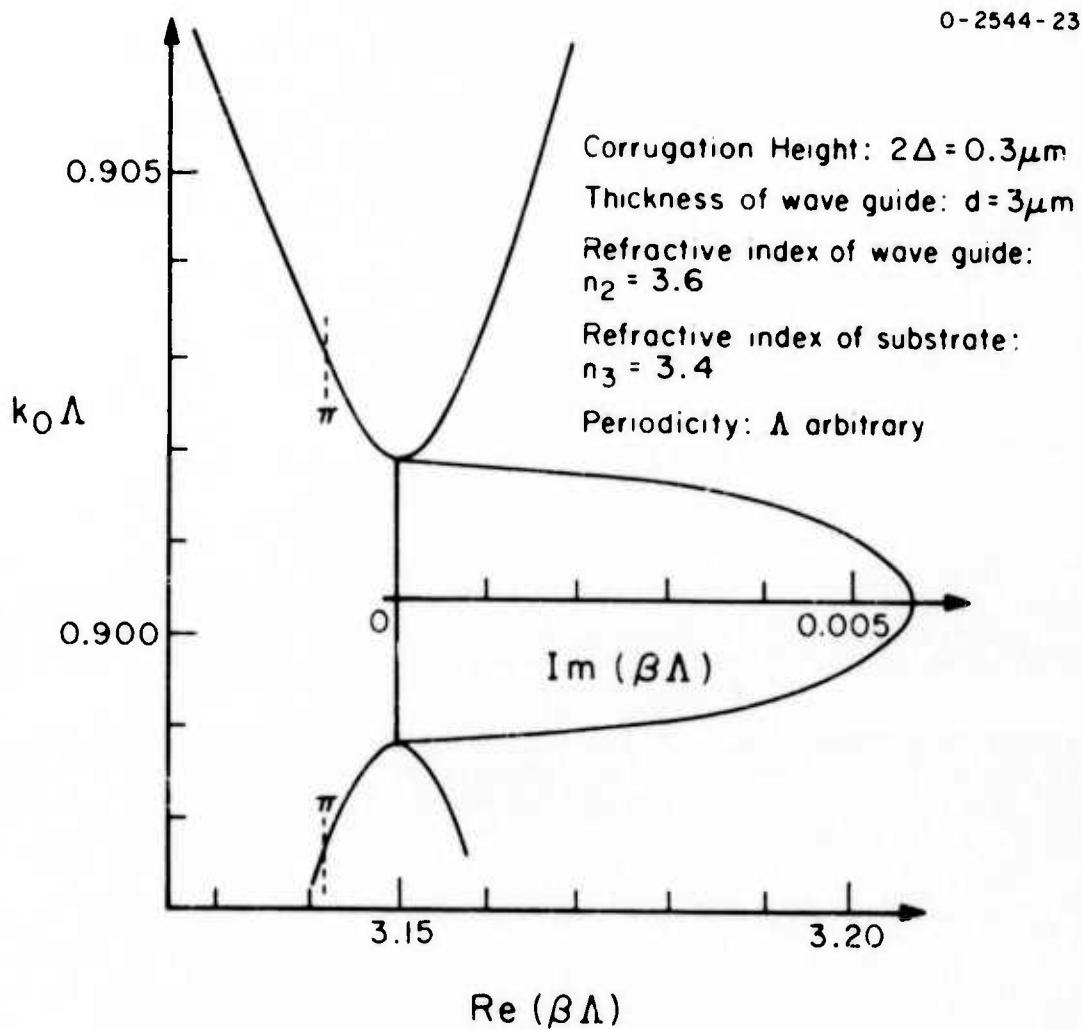
Fig. 29.   Enlarged dispersion diagram at the vicinity
of a forbidden gap (TM mode).

propagation here is dominated by the two modes with $\beta\Lambda = \pm\pi$. This leads us to the coupled mode formalism developed below.[10]

The field component E_x of the corrugated waveguide can be expanded in the TM mode field of the smooth waveguide as

$$E_x = \sum_m \frac{\beta_m B_m(z)}{2\omega\epsilon} H_y^{(m)}(x) \exp\left[i(\omega t - \beta_m z)\right] + c.c., \quad (8)$$

where $B_m(z)$ is the normalized mode amplitude so defined so that $|B_m|^2$ is the total power (per unit width in the y direction) in mode m. The field $H_y^{(m)}(x)$ is given by

$$H_y^{(m)}(x) = -C[(h/\overline{q}) \cos(ht) + \sin(ht)]\exp[p(x+t)], \quad x \leq -t,$$
$$= C[-(h/\overline{q}) \cos(hx) + \sin(hx)], \quad -t \leq x \leq 0,$$
$$= -(h/\overline{q}) C \exp(-qx), \quad x \geq 0, \quad (9)$$

where, referring to Fig. 30, the continuity conditions at $x = 0$ and $x = -t$ result in the eigenvalue relation

$$\tan(ht) = h(\overline{p}+\overline{q})/(h^2 - \overline{p}\overline{q}),$$
$$\overline{p} \equiv (n_2^2/n_3^2)p, \quad \overline{q} \equiv (n_2^2/n_1^2)q. \quad (10)$$

We choose the constant C in eq. (9) so that $|B_m|^2$ is the power per unit width (y) in the mode. This determines C_m as

$$C_m = 2(\omega\epsilon_0/\beta_m t_{eff})^{1/2},$$

where

$$t_{eff} = \frac{\overline{q}^2 + h^2}{\overline{q}^2} \left[\frac{t}{n_2^2} + \frac{q^2 + h^2}{\overline{q}^2 + h^2} \frac{1}{n_1^2 q} + \frac{p^2 + h^2}{\overline{p}^2 + h^2} \frac{1}{n_3^2 p}\right] \quad (11)$$

The effect of surface corrugation is to generate a perturbation polarization wave

$$P_x = \Delta n^2(r) \epsilon_0 E_x, \quad (12)$$

[10] A. Yariv, Jour. Quantum Electronics, to be published.

70
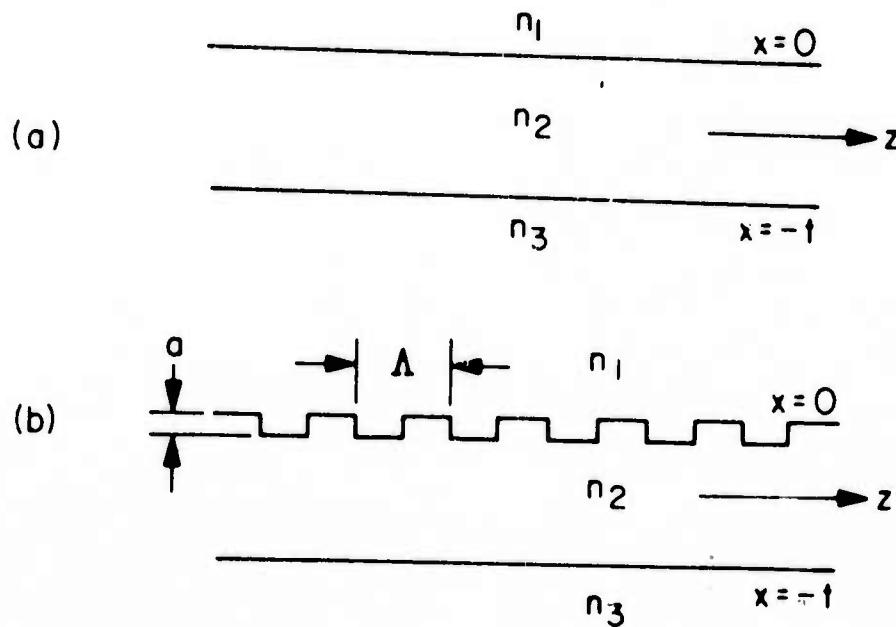
Fig. 30. (a) Unperturbed waveguide. (b) Wave-
guide with square wave perturbation.

where $\Delta n^2(r)$ is the deviation of $n^2(r)$ of the corrugated structure from that of the smooth guide. Referring to Fig. 30(b), we have

$$\Delta n^2(r) = \Delta n^2(x) \left\{ \frac{1}{2} + (2/\pi)\left[\sin \eta z + \frac{1}{3} \sin 3 \eta z + \cdots \right] \right\}$$

$$\Delta n^2(x) = n_2^2 - n_1^2 \quad , \qquad - a \leq x \leq 0 \quad ; \tag{13}$$

$$= 0 \qquad , \qquad \text{elsewhere.}$$

The polarization driving the backward mode is given by eq. (12) when E_x is the field of the forward mode and vice versa. Under these conditions, a substitution of eqs. (8) and (12) into Maxwell's equation leads to

$$dB_m^-/dz = \kappa B_m^+ \exp(-i\Delta z) \quad ,$$

$$dB_m^+/dz = \kappa B_m^- \exp(+i\Delta z) \quad , \tag{14}$$

where the superscripts + and - refer, respectively, to the forward and backward modes. The phase mismatch factor is defined by

$$\Delta(\omega) \equiv 2\beta(\omega) - \eta \quad , \tag{15}$$

where $\eta = 2\pi/\Lambda$ is the fundamental spatial frequency of the periodic modulation. The coupling constant κ is given by

$$\kappa = \frac{\omega\mu_0}{4\pi} \int_{-\infty}^{\infty} \frac{\Delta n^2(x)}{n^2(x)} \left[H_y^{(m)}(x) \right]^2 dx \quad . \tag{16}$$

We consider the case of a wave B_m^+ incident on a corrugated section of length L. The appropriate boundary conditions are $B^-(L) \equiv 0$ and $B^+(0) \equiv B(0)$. The solutions of eq. (14) are then

72

$$B^+(z) = B(0) \frac{\exp\left(+\frac{1}{2} i \Delta z\right)}{-\Delta \sinh\left(\frac{1}{2} SL\right) + iS \cosh\left(\frac{1}{2} SL\right)}$$

$$\times \left\{\Delta \sinh\left[\frac{1}{2} S(z-L)\right] + iS \cosh\left[\frac{1}{2} S(z-L)\right]\right\} . \tag{17}$$

$$B^-(z) = B(0) \frac{2i\kappa \exp\left(-\frac{1}{2} i \Delta z\right)}{-\Delta \sinh\left(\frac{1}{2} SL\right) + iS \cosh\left(\frac{1}{2} SL\right)} \sinh\left[\frac{1}{2} S(z-L)\right]$$

where

$$S \equiv (4\kappa^2 - \Delta^2)^{1/2} . \tag{18}$$

A sketch of the mode power $|B^+|^2$ and $|B^-|^2$ is shown in Fig. 31. The exponential-like decay is caused by backward Bragg scattering and not, as in grating couplers, to radiation. The exponential regime of the solution exists according to eqs. (17) and (18) when

$$\Delta(\omega) \leq 2\kappa . \tag{19}$$

Since $\Delta(\omega) \equiv 2\beta_m(\omega) - \eta$, where $\beta_m(\omega)$ is the propagation constant of the unperturbed m^{th} mode, eq. (17) depends on the frequency ω. It is easy to show that the frequencies at which eq. (19) is satisfied are in the "forbidden" optical gap. From eqs. (8) and (17), we can write the complex propagation constant as

$$\beta' = \beta - \frac{1}{2} \Delta \pm \frac{1}{2} iS = \frac{1}{2} \eta \pm \frac{1}{2} iS . \tag{20}$$

Using the above definitions of Δ and S we have

$$\text{Im}\beta' = \left[\kappa^2 - (\beta-\eta/2)^2\right]^{1/2}$$

$$\simeq \left[\kappa^2 - (n_{eff}^2/c^2)(\omega-\omega_0)^2\right]^{1/2} \tag{21}$$

where ω_0 is the midgap frequency so that $\beta(\omega_0) = \eta/2$. In the second equality of (21) we approximate $\beta(\omega) \simeq (\omega/c)n_{eff}$.

73
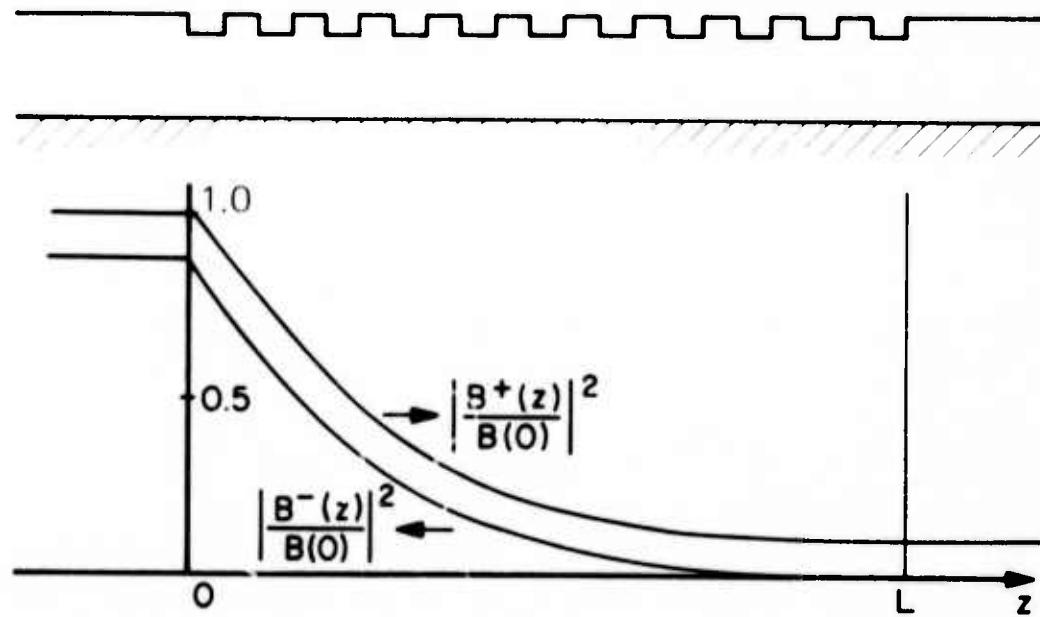
Fig. 31. Normalized mode power flowing in the +z direc-
tion, $(|B^+(z)/B(0)|^2)$ and in the -z direction,
$(|B^-(z)/B(0)|^2)$, as a function of z
$(\kappa L = 1.84, L = 1, \Delta = 0)$.

Thus, c/n_{eff} is the slope of the unperturbed dispersion $(\omega-\beta)$ characteristics near ω_0. The "height" of the energy gap is determined from eq. (21) as

$$(\Delta\omega)_{gap} \equiv \omega_u - \omega_\ell = 2 \kappa c/n_{eff} .\qquad(22)$$

For frequencies ω outside the gap $[\Delta(\omega)^2 > 4\kappa^2]$, $(\beta' - \eta/2)$ $> \kappa$, and β' is real. The shape of the $\omega - \beta'$ curve near the upper limit of the gap $(\omega > \omega_u)$ is obtained from eqs. (18) and (20) as

$$\beta' \approx \frac{1}{2}\eta \pm \left[(n_{eff}^2/c^2) (\omega-\omega_u)^2 + (2n_{eff}\,\kappa/c)(\omega-\omega_u) \right]^{1/2} .\qquad(23)$$

Equations (21), (22), and (23) are general and apply to any spatially periodic perturbation. As a check on the above theory we applied it to the same situation considered in the first part of this section. For the case of well confined modes, eq. (16) simplifies to

$$\kappa \approx \frac{\lambda_0 a}{6n_2 t^3}\qquad(24)$$

where $a \ll \lambda_0$. We have plotted eqs. (21) and (23) using the same data as in Fig. 29, i.e., $t = 3$ μm, $\Lambda = 0.143$ μm, $\lambda_0 = 1$ μm, $a = 0.3$ μm, $n_3 = 3.4$, $n_2 = 3.6$, $n_1 = 1$ and took $n_{eff} \simeq n_2$. The result is shown in Fig. 32. The agreement is close. At least part of the discrepancy is a result of the under-estimation of κ which resulted from the well-confined mode approximation. The above agreement shows that we can use eqs. (17), (21), (22), and (23) in designing new Bragg filters and modulators.

The operation as modulators is based on the fact that the transmission coefficient of the device

$$|B^+(L)/B(0)|^2 \simeq \exp\left\{ -2\left[\kappa^2 - (\beta-\eta/2)^2 \right]^{1/2} L \right\} .$$
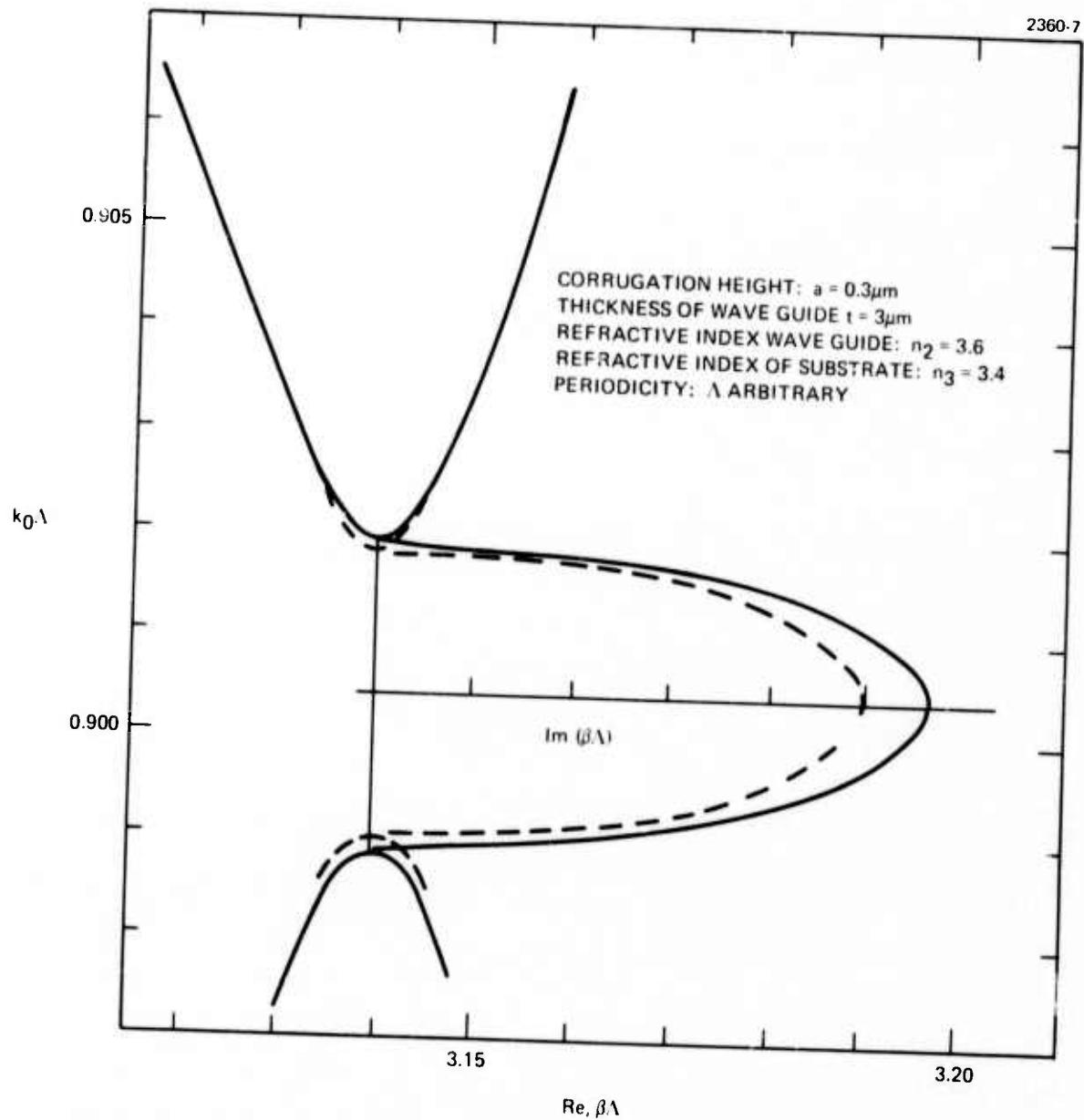
Fig. 32. Dispersion diagram for periodically perturbed wave-
guide in the region of the forbidden optical gap.

Since $\beta \sim (\omega/c)n_2$, the transmission depends on either ω, as described above, or on n_2. An electro-optic (or photoelastic) variation of n_2 will vary the transmission. Referring to Fig. 32, the effect of varying n_2 can be understood by fixing the frequency but moving the dispersion diagram vertically. In the limit of well confined modes the expression (eq. 24) for κ is also valid for TE modes. The resulting transmission and reflection characteristics are shown in Fig. 33 in which $\kappa L = 1.84$.

O-2544-26
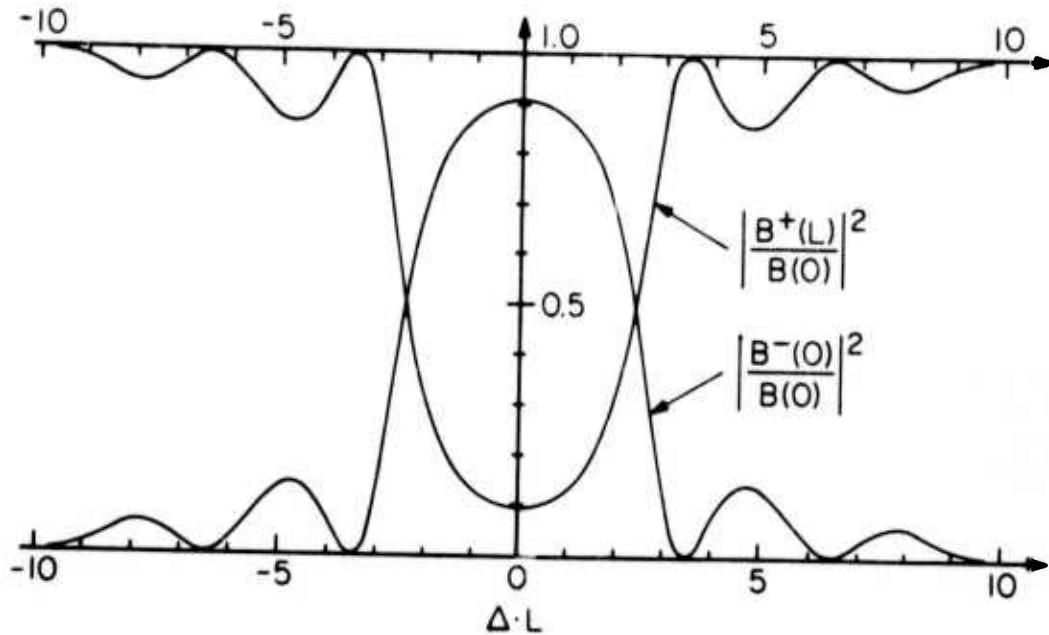
Fig. 33. The transmission and reflection characteristics of a corrugated section of length L as a function of $\Delta \cdot L$ drawn for $\kappa L = 1.84$.

VI.   FUTURE PLANS

The work on this program is expected to continue along the lines established by the work performed to date. The basic assumptions and numerical values of various parameters which were used in the material requirements calculations will be verified by actual measurements on the materials grown in the course of the program. The calculations will then be refined and performed accurately. One of the most important properties of $Ga_{1-x}Al_xAs$ to be accurately established is its absorption in the vicinity of the band edge as a function of Al concentration.

The three epitaxial techniques will be used to produce waveguide structures. The infinite melt method will provide large area films of $Ga_{1-x}Al_xAs$ of varying aluminum compositions for use as substrates. Lack of large area substrates of device quality and homogeneity which has been the major bar to the fabrication of acceptable waveguides, now seems to be overcome.

The limited melt slide-bar technique will be used to grow thin layers of $Ga_{1-x}Al_xAs$ on the substrates from the infinite method. The aluminum concentration in these layers will be adjusted to be 2 to 3% lower than in the substrates. These multilayer structures will be examined by electron microprobe and photoluminescence techniques to determine the aluminum composition profile in these structures and their guiding properties will be correlated with these measurements.

The vapor phase epitaxy will be used to grow thin layers of n-type GaAs with low carrier concentration on $Ga_{0.96}Al_{0.04}As$ layers to determine their usefulness as waveguides. At a later stage such structures also will be used to fabricate other integrated optics elements.

As the waveguide structures become available the optical propagation characteristics such as loss, dispersion and field profiles of the films will be measured. Experimental setups to perform all these measurements are being perfected using the waveguides presently available.

The device elements task will continue exploring the relationship between the device requirements and material properties. The theoretical work on periodic waveguides will be pursued further by considering specific systems such as the $GaAs-Ga_{1-x}Al_xAs$ waveguides presently grown under the contract. The intent is to generate specific design data which will enable us, for example, to design an optical filter for a specific wavelength region using given waveguide materials and dimensions. We will also begin planning specific experiments for testing the theory and for evaluating the feasibility of optical filters.

REFERENCES

1. J.T. Boyd, IEEE J. Quantum Electron. QE-8, 788 (1972).

2. J. Shah, B. Miller, and A. DiGiovanni, J. Appl. Phys. 43, 3436 (1972).

3. M.D. Sturge, Phys. Rev. 127, 768 (1962).

4. E.A.J. Marcatili, Bell Syst. Tech. J. 48, 2103 (1969).

5. S. Somekh, E. Garmire, A. Yariv, H.L. Garvin, and R.G. Hunsperger, Appl. Phys. Lett. 22, 46 (1973).

6. K. Sakuda and A. Yariv, Optics Communications 8, 1 (1973).

7. H. Stoll and A. Yariv, Optics Communications 8, 5 (1973).

8. H.L. Garvin, E. Garmire, S. Somekh, H. Stoll, and A. Yariv, Appl. Optics 12, 455 (1973).

9. H. Yen, et al., to be published in Optics Communications.

10. A. Yariv, Jour. Quantum Electronics; to be published.